

Review

Perovskite-Based Catalysts as Efficient, Durable, and Economical NO_x Storage and Reduction Systems

Jon A. Onrubia-Calvo , Beñat Pereda-Ayo and Juan R. González-Velasco *

Chemical Technologies for Environmental Sustainability TQSA, Department of Chemical Engineering, Faculty of Science and Technology, University of the Basque Country UPV/EHU, Barrio Sarriena s/n, Leioa, 48940 Bizkaia, Spain; jonander.onrubia@ehu.eus (J.A.O.-C.); benat.pereda@ehu.eus (B.P.-A.)

* Correspondence: juanra.gonzalezvelasco@ehu.es

Received: 17 January 2020; Accepted: 7 February 2020; Published: 9 February 2020



Abstract: Diesel engines operate under net oxidizing environment favoring lower fuel consumption and CO₂ emissions than stoichiometric gasoline engines. However, NO_x reduction and soot removal is still a technological challenge under such oxygen-rich conditions. Currently, NO_x storage and reduction (NSR), also known as lean NO_x trap (LNT), selective catalytic reduction (SCR), and hybrid NSR–SCR technologies are considered the most efficient control after treatment systems to remove NO_x emission in diesel engines. However, NSR formulation requires high platinum group metals (PGMs) loads to achieve high NO_x removal efficiency. This requisite increases the cost and reduces the hydrothermal stability of the catalyst. Recently, perovskites-type oxides (ABO₃) have gained special attention as an efficient, economical, and thermally more stable alternative to PGM-based formulations in heterogeneous catalysis. Herein, this paper overviews the potential of perovskite-based formulations to reduce NO_x from diesel engine exhaust gases throughout single-NSR and combined NSR–SCR technologies. In detail, the effect of the synthesis method and chemical composition over NO-to-NO₂ conversion, NO_x storage capacity, and NO_x reduction efficiency is addressed. Furthermore, the NO_x removal efficiency of optimal developed formulations is compared with respect to the current NSR model catalyst (1–1.5 wt % Pt–10–15 wt % BaO/Al₂O₃) in the absence and presence of SO₂ and H₂O in the feed stream, as occurs in the real automotive application. Main conclusions are finally summarized and future challenges highlighted.

Keywords: lean-burn engines exhaust control; NO_x removal; NO_x storage and reduction; perovskite-based catalysts; sulfur resistance; hydrothermal resistance

1. Introduction

The concern about pollutants released by internal combustion engines has increased significantly since the late 1900s. Currently, with more than 600 million automobiles worldwide, vehicle exhaust is one of the main causes of air pollution, especially in urban areas. Unburned hydrocarbons (HCs), carbon monoxide (CO), particulate matter (PM), sulfur oxides (SO_x), nitrogen oxides (NO_x), and soot are the main pollutants in the exhaust [1]. However, exhaust composition depends on the engine operation principle. In this sense, two types of engines can be differentiated, gasoline engines and diesel or lean-burn gasoline engines. The latter operate with high air-to-fuel ratios (A/F = 20–65), which favors fuel economy, engine efficiency, driving performance, and limits CO₂, CO, and HCs emissions with respect to stoichiometric gasoline engines. These advantages have motivated the increasing implementation of diesel or lean-burn engines during the last years [2]. Nevertheless, the excess of oxygen introduced leads to a net oxidizing environment, which limits the simultaneous removal of NO_x and soot [3]. As a result, the control of NO_x, PM and soot is still a technological challenge in diesel and lean-burn gasoline engines. This fact, together with the progressive implementation of

stringent standards regarding NO_x and soot emissions (currently Euro VI legislation in Europe), has driven the development of a complex exhaust treatment system. The system is usually composed of diesel oxidation catalyst (DOC) followed by a diesel particulate filter (DPF) and NO_x reduction catalyst (NRC) in series. This system is usually complemented by ammonia slip catalyst (ASC) placed downstream [4]. The limited NO_x reduction efficiency of diesel engines has driven that recent efforts have been mainly focused on the development of an efficient NRC. NO_x storage and reduction (NSR), selective catalytic reduction (SCR), and the hybrid NSR–SCR technologies have been developed in order to mitigate NO_x emissions in diesel engines [5].

NO_x storage and reduction (NSR) technology was introduced by Toyota in the mid-1990s [6]. This alternative operates cyclically under fuel-lean and fuel-rich conditions. The duration of the former period is in the order of few minutes while the latter period duration is few seconds. During the long lean period NO_x are trapped over catalytic surface. Then, in the subsequent short-rich period, stored NO_x are reduced preferentially to N_2 . For that, the NSR catalyst compositions usually contain active sites for NO -to- NO_2 oxidation and NO_x -to- N_2 reduction, as well as storage components for NO_x adsorption during lean period [7–9]. In this context, Pt–Ba/ Al_2O_3 catalyst emerges as the model NSR formulation [10,11]. Alternatively, SCR technology achieves NO_x reduction under steady oxidizing conditions by the injection of a selective chemical reductant of the NO_x . The ammonia generated from urea decomposition, which is stored on-board in a specific reservoir is the usual reductant in this technology (NH_3 -SCR) [12,13]. In this case, catalysts based on Cu or Fe exchanged on different zeolites are widely adopted as NH_3 -SCR formulation [14–16].

Both alternatives, the NSR technology and the SCR technology, show some drawbacks that limit their extended implementation, as summarized in Table 1. On the one hand, NSR system requires high Pt loads (1–2 wt %) which increase the costs and limits the hydrothermal and sulfur resistance. Furthermore, some extent of NH_3 and N_2O may be formed during the short-rich period. On the other hand, NH_3 -SCR involves a continuous admission of NH_3 to reduce NO_x , which is formed from the thermal decomposition of urea stored in on-board tank. This fact limits the implementation of SCR technology in small vehicle due to the cost and space requirement. Taking into account that NSR system generates some NH_3 as byproduct during the rich phase, a reasonable interest in linking both technologies has grown. Hybrid NSR–SCR technology emerges as a potential solution of some of the main drawbacks previously reported for stand-alone NSR and SCR technologies [17]. Specifically, in the hybrid NSR–SCR system the NO_x removal efficiency is increased notably with a simultaneous decrease in the NH_3 slip. This operation principle allows circumventing the implementation of an on-board NH_3 generation unit. The coupled NSR–SCR technology is composed of NSR and SCR catalysts operating cyclically in a similar way to single-NSR technology. SCR catalyst can be placed downstream of the NSR catalyst in sequential NSR–SCR configuration or alternatively in a single-brick composing the dual-layer architecture. In most cases, the NO_x removal efficiency of hybrid NSR–SCR systems has been analyzed using model NSR formulation ((1–2 wt %) Pt–(10–15 wt %) BaO/ Al_2O_3). However, the amount of noble metal (Pt) should be reduced or replaced by less expensive and thermally more stable materials.

Taking into account these drawbacks, during the last decade, a great interest in developing perovskite-based formulation for NO_x removal in diesel engines has grown. Particularly, high structural stability and low cost qualify perovskite oxides as potential alternative to Pt-based catalysts, widely implemented as model NSR formulations [18]. Therefore, the main objective of this review is to overview the recent progress in the application of perovskite-based materials in the stand-alone NSR and combined NSR–SCR systems. First, we shall focus on the general application of perovskite-based formulations to NO_x removal in diesel engines. Then, a general outlook on different preparation methods and chemical compositions used during the application of the perovskite-based formulation to the single-NSR system is provided. A major emphasis is devoted to the viability of perovskite-based formulation as alternative to Pt-based NSR catalyst. For that, the thermal and sulfur resistance of

both type formulations is also compared. Finally, a brief look of the viability of the perovskite-based formulations as NSR system in the combined NSR–SCR technology is included.

Table 1. Comparison among stand-alone NSR, stand-alone SCR, sequential NSR–SCR, and dual layer NSR–SCR technologies for NO_x removal in diesel light-duty vehicles (adapted from [17] with permission of Wiley-VCH)

	NSR	SCR	NSR + SCR	NSR–SCR
Principle	The system runs under lean-rich cycles. During lean period NO _x is adsorbed on the catalyst, and then is released and reduced in the subsequent rich period.	The SCR catalyst reduces selectively NO _x with NH ₃ generated from an aqueous urea solution.	Operates similarly to NSR system. The SCR unit downstream reduces the NO _x with the NH ₃ produced in the NSR.	Similar operation to NSR system. The NO _x diffuses the top SCR layer and generates NH ₃ in the bottom NSR layer, which then reduces the NO _x slipped from the NSR.
Model catalyst	Pt–Ba/Al ₂ O ₃ deposited on a cordierite monolith.	Cu, Fe/Chabazite deposited on a cordierite monolith.	Sequential NSR + SCR double monolith.	Dual layer NSR + SCR single monolith.
Advantages	70–90% efficiency at low loads. More economical for light-duty vehicles. Reductant fluid not required.	Up to 90% NO _x conversion efficiency. More economical for heavier vehicles.	High NO _x removal efficiency at low temperatures. Reduction of PGM. Reductant fluid not required.	High NO _x removal efficiency at low temperatures. Less volume and weight than sequential monoliths.
Limitations	Limited NO _x storage capacity and NSR efficiency for highway and ascending driving. Need of high amount of PGM.	Low sulfur resistance. Requires on board DEF AdBlue storage tank with heating and injection system. Operational limitations under urban driving conditions.	High cost. Packaging constrains (double monolith). Possible migration of Pt from NSR to SCR. Calibration difficulties.	High cost. Spillover of stored NH ₃ onto vicinal Pt sites, which limits NO _x reduction. Possible migration of Pt from NSR to SCR layer. Calibration difficulties due to its complexity.

2. Perovskite-Based Catalysts in Automotive Exhaust Catalytic Converters

Perovskite-type oxides have attracted attention as promising catalyst for exhaust control in automotive applications since Libby [19] and Voorhoeve et al. [20] explored perovskites firstly in early 1970s. The term of perovskite is the general name for oxides with ABO₃ and/or A₂BO₄ structure. In the ideal cubic crystalline unit cell of perovskite (Figure 1), the larger cation A is located in the center edge of the structure; meanwhile the smaller cation B is located in the center of the octahedron. O is an anion that bonds both cations [21]. A cation (coordinated by 12 oxygen), can be a rare earth, alkaline, or alkaline-earth cation. The B cation (surrounded by six oxygen in octahedral coordination) can be any transition metal ions from 3d, 4d, or 5d configuration. In the perovskite structure, A cation plays an essential role as responsible for the stabilization of the structure, while B cation is responsible for the catalytic activity.

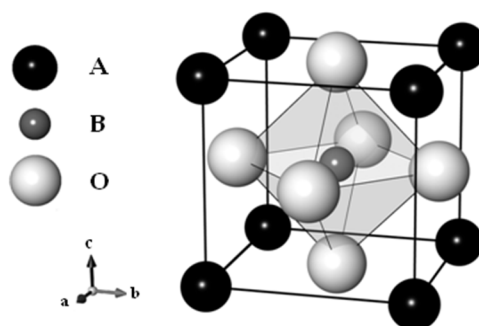


Figure 1. Ideal crystal structure of perovskite oxides with ABO₃ composition.

Perovskite-type oxides can accommodate a wide number of components in A and B sites and can stabilize various distorted structures. The wide range of possible cationic substitutions in the perovskite family generates great flexibility in terms of structure, allowing it to be adjusted appropriately to the process. The stability of the perovskite structure is governed by geometric considerations summarized by the Goldschmidt tolerance factor, Equation (1),

$$t = \frac{r_A + r_O}{\sqrt{2}(r_B + r_O)} \quad (1)$$

where r_A , r_B , and r_O are the respective radii of A, B and oxygen ions. The tolerance factor must be in the range of 0.75 to 1.00 so that the oxide can crystallize with perovskite-type structure.

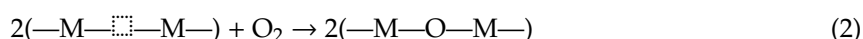
As above mentioned, the flexibility to modulate the catalytic properties of the perovskite structure by the partial or total substitution of A and B cations allows to better adapting to the desired automotive applications [18,22]. Indeed, perovskite-based materials have been widely implemented as low-cost alternative to the catalysts composed of platinum-group metals (PGMs) in automotive catalytic converters [19,20,23,24]. Perovskites have shown excellent activity in oxidation reactions in their implementation as diesel oxidation catalyst (DOC) [23,25–32]. Furthermore, these oxides demonstrated excellent efficiency in the joint mitigation of NO_x and soot emissions from diesel engines. Thus, these materials have been implemented in diesel particulate NO_x reduction filter (DPNR) [33–39]. On the other hand, the catalytic decomposition of nitrous oxide or nitric oxide has been reported as a one their potential applications [40–46]. Finally, perovskites have been widely implemented for NO_x reduction in both stoichiometric gasoline engines (three-way catalyst, TWC) [33,47–53] and diesel or lean-burn gasoline engines (NSR and SCR systems). Recently, the latter application has gained special attention due to the increasing necessity of developing an efficient NO_x reduction system in diesel engines. This fact became more evident for NSR alternative to overcome the requirement of high platinum-group metals (PGMs) loads to maximize NO_x removal efficiency. Therefore, a great range of studies have focused on developing perovskite-based formulations as economical and more durable alternative to Pt-based model catalyst.

3. Perovskite-Based Catalysts for NSR Technology

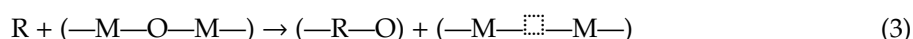
NSR technology is considered as a promising approach to control NO_x emissions in diesel engines. This alternative operates cyclically under fuel-lean and fuel-rich conditions. During the lean period, platinum oxidizes NO-to- NO_2 , which is then adsorbed over Ba in the form of nitrites/nitrates. During the subsequent short-rich period, a reductant, such as CO, H_2 , or HC, is used to release and reduce the stored NO_x . Thus, NO-to- NO_2 conversion is considered a critical step in improving the NO_x removal efficiency in the model NSR formulation. However, this reaction requires high Pt loadings, compound very costly and with limited thermal stability [23]. As a result, the applicability of perovskites-based materials to NSR technology is initially related to the capacity to oxidize NO-to- NO_2 during the lean period. After that, the NO_2 form should be efficiently trapped over catalytic surface during the oxidizing period. Finally, the perovskite-based catalyst should selectively reduce the stored- NO_x -to- N_2 . In order to cover efficiently the consecutive stages in the NSR process different alternatives have progressively been explored. Some authors modified the physicochemical properties of the perovskites-based formulations by partial substitution of A and B cations. Alternatively, other studies supported perovskites over high surface area materials, whereas in other cases additional components were incorporated over perovskite-based formulations. This allows tailoring the catalytic properties of perovskite-based materials for automotive applications. The final goal is to develop a perovskite-based formulation with similar or even higher NO_x removal efficiency, with more sulfur resistance and hydrothermal stability than the Pt-based model catalyst.

3.1. NO-to-NO₂ Conversion

As previously discussed, NO₂ plays a decisive role as an intermediate species in the NSR process. Thus, a primary prerequisite to explore the real applicability of perovskite-oxides to NSR technology is to develop a perovskite-based formulation with high NO oxidation capacity. Generally speaking, Choi et al. [54] reported that the catalytic activity in oxidation reactions is strongly influenced by molecular and atomic interactions of oxygen with the perovskite surface. In this sense, many authors suggested that the catalytic oxidation over metal oxides (M) follows a Mars–van Krevelen mechanism [55,56]. As a result, the adsorption of dissociated oxygen is facilitated by vacancies (□) in the oxide lattice as schematizes the following reaction



then, the regeneration of the oxygen vacancies takes place by the reduction of the oxide with a reductant (R) to complete the catalytic cycle,



In order to obtain a formulation with high NO oxidation capacity, different preparation methods and perovskite compositions have been prepared and tested, as summarized in Table 2. Co-precipitation and especially citric acid method are the more explored synthesis routes due to their simplicity, ease of scale-up, and appropriate textural properties [22]. The synthesis conditions—such as citrate to nitrate molar ratio in the starting solution, pH of the gel precursor dissolution, and calcination protocol—have shown significant influence on NO-to-NO₂ conversion activity of the material prepared by citric acid method [25,57]. Regarding perovskite composition, LaCoO₃ and LaMnO₃ perovskites and their doped modifications have been investigated extensively for NO-to-NO₂ conversion due to the excellent performance on other oxidation reactions [58,59].

On the developed formulations, at low temperatures, low conversions were attained, due to kinetic limitations. With increasing temperatures NO-to-NO₂ conversion began to increase until 300–350 °C, where the conversion began to drop due to thermodynamic limitations and the reaction pathway then followed the equilibrium curve, as observed in Figure 2. Both LaCoO₃ and LaMnO₃ benchmark systems show excellent NO-to-NO₂ conversion efficiencies [58]. Based on the Mars–van Krevelen mechanism above described (Equations (2) and (3)), the excellent activity of these materials for oxidation reactions can be related to some specific structural properties, such as change of oxidation state of B cation, active oxygen mobility, and ion vacancy defect [59]. Indeed, the promotion of oxygen vacancy density seems to be the key factor to maximize oxidation efficiency [60–64]. La³⁺ partial substitution by Ca²⁺, Ba²⁺, or Sr²⁺, is accepted as a simple way to alter the main physico-chemical properties of perovskite (crystallinity, average crystal size, specific surface area, and redox properties). Among them, Sr²⁺ is the most explored cation for this approach. The introduction of lower oxidation state Sr²⁺ in substitution of La³⁺ in LaMnO₃ and LaCoO₃ lattice generates a net charge imbalance that may be compensated by alteration of the oxidation state of a fraction of transition metal, leading to Mn⁴⁺ or Co⁴⁺ formation.

Table 2. Activity in NO-to-NO₂ oxidation of different perovskite-based formulations

Formulation	Shape	Feedstream	GHSV, h ⁻¹	T, °C	X _{NO-to-NO₂} , %	Ref.
LaCoO ₃	powder	[NO] = 100 ppm; [O ₂] = 10%	30,000	260	83.0	[58]
LaCoO ₃ ⁽⁺⁾	powder	[NO] = 400 ppm; [O ₂] = 5%	80,000	350	57.9	[65]
La _{0.9} Sr _{0.1} CoO ₃	monolith	[NO] = 400 ppm; [O ₂] = 8%	30,000	300	86.0	[23]
La _{0.7} Sr _{0.3} CoO ₃	powder	[NO] = 800 ppm; [O ₂] = 5%	80,000	300	74.1	[66]
La _{0.7} Sr _{0.3} CoO ₃	powder	[NO] = 650 ppm; [O ₂] = 6%	123,500	300	80.0	[25]
La _{0.7} Sr _{0.3} Co _{0.97} Pd _{0.03} O ₃	powder	[NO] = 500 ppm; [O ₂] = 6.7%	32,000	280	87.8	[67]
La _{0.7} Sr _{0.3} Co _{0.8} Fe _{0.2} O ₃	powder	[NO] = 750 ppm; [O ₂] = 5%	80,000	300	84.6	[68]
La _{0.5} Sr _{0.5} CoO ₃	powder	[NO] = 500 ppm; [O ₂] = 3%	120,000 ^(a)	300	55.0	[69]
La _{0.9} Ba _{0.1} CoO ₃	powder	[NO] = 400 ppm; [O ₂] = 10%	180,000 ^(a)	265	93.0	[26]
La _{0.8} Ce _{0.2} CoO ₃	powder	[NO] = 800 ppm; [O ₂] = 8%	0.096 ^(b)	300	80.0	[28]
LaCo _{0.92} Pt _{0.08} O ₃	powder	[NO] = 280 ppm; [O ₂] = 8%	72,000	300	< 80.0 ^(*)	[70]
LaCo _{0.9} Cu _{0.1} O ₃	powder	[NO] = 400 ppm; [O ₂] = 10%	180,000 ^(a)	310	82.0	[71]
LaNi _{0.7} Co _{0.3} O ₃	powder	[NO] = 400 ppm; [O ₂] = 6%	200,000	325	< 80.0	[27]
LaMnO ₃	monolith	[NO] = 400 ppm; [O ₂] = 8%	30,000	350	62.0	[72]
La _{0.9} MnO ₃	powder	[NO] = 100 ppm; [O ₂] = 10%	30,000	296	85.0 ^(*)	[59]
La _{0.9} Sr _{0.1} MnO ₃	powder	[NO] = 650 ppm; [O ₂] = 6%	123,500	325	65.0	[25]
La _{0.9} Sr _{0.1} MnO ₃	monolith	[NO] = 400 ppm; [O ₂] = 8%	30,000	350	62.5	[23]
La _{0.7} Sr _{0.3} MnO ₃	powder	[NO] = 800 ppm; [O ₂] = 5%	80,000	350	70.2	[57]
La _{0.9} Ca _{0.1} MnO ₃	powder	[NO] = 100 ppm; [O ₂] = 10%	30,000	300	82.0	[73]
La _{0.8} Ag _{0.2} MnO ₃	powder	[NO] = 400 ppm; [O ₂] = 8%	600,000	250	~ 90.0 ^(*)	[74]
LaMn _{0.9} Co _{0.1} O ₃	powder	[NO] = 100 ppm; [O ₂] = 10%	n.a.	300	76.5	[29]
BaTi _{0.8} Cu _{0.2} O ₃	powder	[NO] = 500 ppm; [O ₂] = 6%	n.a.	400	47.0	[75]

(*) Presence of H₂O and/or CO₂. (+) Prepared by nanocasting. (a) Units (mL g⁻¹ h⁻¹). (b) Units (g s mL⁻¹).

Alternatively, the oxidation state of transition metal could be maintained unaltered (Mn³⁺ or Co³⁺), but instead oxygen vacancies could be generated in the lattice to attain the charge balance. Even a mixed situation showing altered oxidation state of transition metal along with oxygen vacancies in the lattice could be expected. As suggested by Kim et al. [23] and more recently in our study [25] charge imbalance associated to strontium (Sr²⁺) incorporation in the perovskite lattice in substitution of lanthanum (La³⁺) was preferentially balanced by Mn⁴⁺ promotion in La_{1-x}Sr_xMnO₃ perovskites, whereas formation of oxygen vacancies seems to be the mechanism for charge compensation in La_{1-x}Sr_xCoO₃ perovskites, where Co remained as Co³⁺ ions. The preferential formation of oxygen vacancies explains the higher

NO-to-NO₂ conversion efficiencies for La_{1-x}Sr_xCoO₃ perovskites (Figure 2). Indeed, the designed perovskite-based materials could potentially rival Pt-based model catalyst (Pt-Ba/Al₂O₃). Thus, La_{1-x}Sr_xMnO₃ and La_{1-x}Sr_xCoO₃ perovskites can be considered efficient approaches to promote NO-to-NO₂ conversion in automotive catalysis.

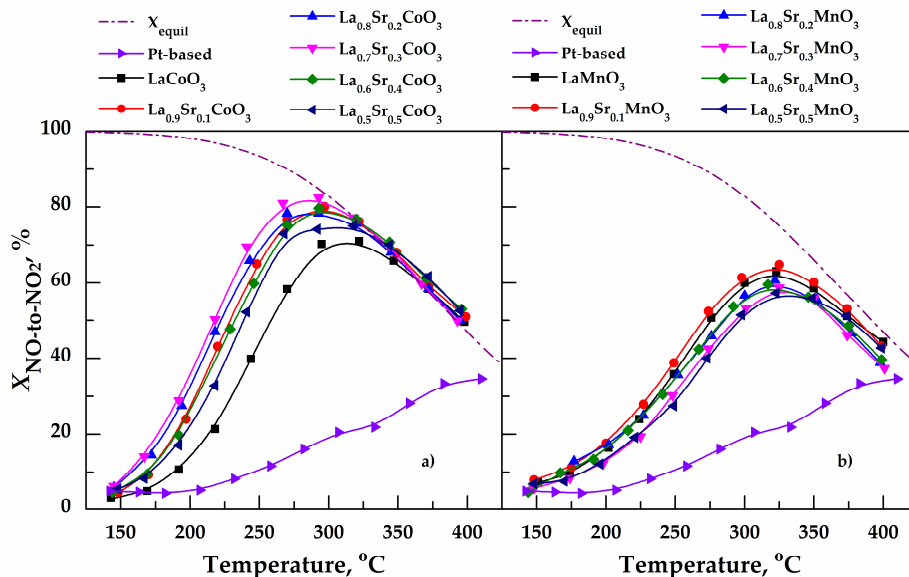


Figure 2. NO-to-NO₂ oxidation capacity of (a) La_{1-x}Sr_xCoO₃ and (b) La_{1-x}Sr_xMnO₃ perovskites with x ranging from 0 to 0.5, together with a model Pt-based catalyst. Reprinted from [25]. Copyright (2017) Elsevier.

Different authors carried out kinetic studies on NO-to-NO₂ oxidation process with LaMnO₃ and LaCoO₃-type perovskites. The results obtained lead to similar conclusions. On the one hand, reaction rate could be linearly accelerated by increasing the concentration of NO and O₂ [57], whereas the NO oxidation rate of LaMnO₃ and LaCoO₃-type perovskites is limited in the presence of NO₂ [54,72,74]. Indeed, Constantinou et al. [76] determined a NO, O₂, and NO₂ orders near to 1, 1 and -1, respectively for LaMnO₃ perovskite. Regarding the apparent activation energies of these materials, their values were in the range of 31–45 kJ/mol for La_xMnO₃ perovskites and in the range of 50–100 kJ/mol for La_{1-x}Sr_xCoO₃ perovskites.

Some of the studies reported in Table 1 have been focused on understanding the electronic structure of perovskites [54,69,71]. Specifically, Density Functional Theory (DFT) calculations have been carried out to analyze the NO-to-NO₂ reaction on LaCoO₃-type perovskites. These studies try to develop theoretical model to describe oxygen exchange process during NO-to-NO₂ oxidation. Indeed, they concluded that the NO-to-NO₂ reaction is favored by Cu [71] or Sr [54] doping due to a decrease of the energy of extralattice oxygen, favoring oxygen vacancies formation. Furthermore, as observed by kinetic experiments, the formation of NO₂ seems to limit NO oxidation.

3.2. NO_x Adsorption under Oxidizing Conditions

Once NO is oxidized to NO₂, the nitrogen dioxide formed should be efficiently trapped over the catalytic surface. In agreement with above described, A-site elements of perovskite are usually alkali/alkaline earth metals, which serve as ideal adsorption sites for the NO_x storage. As a result, perovskite-type oxides were also implemented as efficient lean NO_x trap materials. For the first time in the scientific literature, Hodjati et al. [77–79] reported the NO_x storage capacity (NSC) of different perovskite-type catalysts (with A = Ca, Sr or Ba; and B = Sn, Zr or Ti). Their studies showed that for the A-site cations NSC was in the order of Ca > Sr > Ba; while the influence of the B-site cations on the NSC was in the order of Ti > Zr > Sn. Thus, the BaSnO₃ perovskite had the largest NO_x storage capacity.

In a series of consecutive studies BaCoO₃ [80,81] and BaFeO₃ [82–84] perovskites were also explored as alternatives with high NO_x storage capacity and notable sulfur resistance. In these materials, the presence of BaCO₃ as an impurity promoted the NO_x adsorption capacity; however, this phase limited the regeneration capacity after SO₂ poisoning. More recently, perovskites BaFe_{0.8}Ti_{0.2}O₃ [85] and BaFe_{0.8}Cu_{0.2}O₃ [75,86] have been proposed as alternative formulations.

Alternatively, La-based perovskites have been extensively studied in recent years due to their excellent NO oxidation conversion and structural stability. As observed for NSR model catalysts, La-based perovskites show volcano-type dependence of the NO_x storage capacity with temperature, showing maximum NSC around 350–400 °C. At higher temperatures, NO_x adsorption capacity tends to decrease due to the lower stability of NO_x adsorbed species together with the lower NO-to-NO₂ conversion (Figure 2), which is the limiting step during the NO_x storage step. In agreement with that observed for NO oxidation capacity, the modification of physicochemical properties by the partial substitution of A and B cations could promote NO_x adsorption efficiency. In this case, La³⁺ was partially substituted by other cations with high basicity, such as K⁺, Ca²⁺, Ba²⁺, or Sr²⁺, due to their high NO_x adsorption capacity in the conventional NSR formulations. In fact, some studies demonstrated that Sr²⁺ rather than La³⁺ cations preferred to migrate from the bulk to the surface during the NO_x storage period. This migration enhanced the perovskite NSC and catalytic performance due to the presence of higher amount of basic sites at the surface [87–89]. Similar process can be expected for the other explored cations. Ueda et al. [90] observed that the partial replacement of 30% of La³⁺ by Ba²⁺ practically tripled the NO_x storage capacity of perovskite LaFe_{0.97}Pd_{0.03}O₃. Meanwhile, Li et al. [34] proposed the La_{0.9}K_{0.1}Co_{0.9}Fe_{0.1}O_{3-δ} perovskite as lean NO_x trap material. More recently, Li et al. [66] observed how doping LaCoO₃ perovskite with 30% of Sr (La_{0.7}Sr_{0.3}CoO₃) maximized the storage capacity of La_{1-x}Sr_xCoO₃ perovskites. The best NO_x adsorption efficiency was assigned to a best balance between NO-to-NO₂ oxidation efficiency and NO_x adsorption sites concentration at the surface. Based on the results of DRIFT, they also proposed three main storage routes in these solids: monodentate nitrates (1440 cm⁻¹), free nitrate ions (1384 cm⁻¹), and nitrates in perovskite (1362 cm⁻¹). An increase in temperature above 300 °C favors the storage of NO_x as free nitrate ions formed on strontium carbonates or surface structural strontium, as well as the adsorption of the other two species (Figure 3).

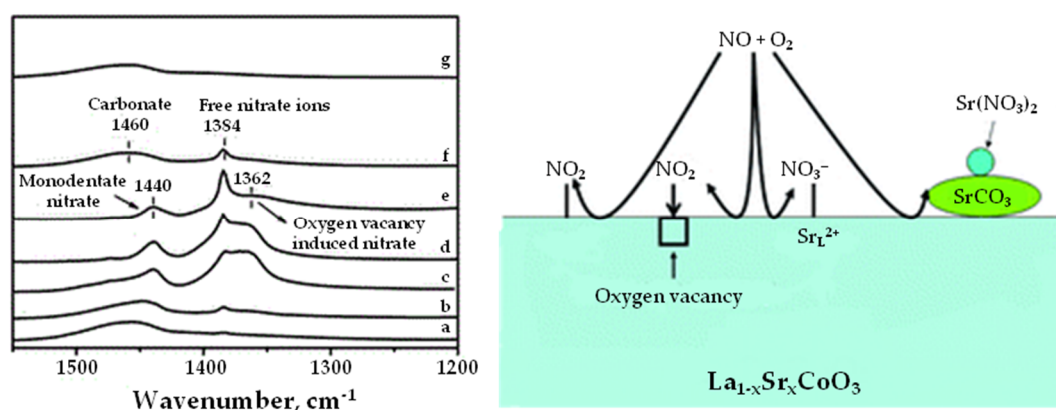


Figure 3. FT-IR spectra (left side figure) of La_{0.7}Sr_{0.3}CoO₃: fresh (a); after NO_x storage at 200 °C (b); 250 °C (c); 300 °C (d); 350 °C (e); and 400 °C (f); the sample (c) reduced by 5% H₂ at 300 °C for 10 min (g). Possible NO_x storage routes (right side figure) on La_{1-x}Sr_xCoO₃ perovskites. Adapted from [66]. Copyright (2011) The Royal Society of Chemistry.

López-Suarez et al. [91] observed similar NO_x storage mechanism for the SrTi_{0.89}Cu_{0.11}O₃ perovskite. Otherwise, Dong et al. [57] analyzed the influence of synthesis conditions on the NO_x storage capacity of perovskites La_{0.7}Sr_{0.3}MnO₃. In this case they observed that the adsorption of NO_x at 350 °C occurs mainly in the form of free nitrate ions, which is favored by a greater specific

surface area and a more homogeneous distribution of the different components. As described for NO oxidation conversion, the synthesis conditions also influence the NO_x adsorption capacity of these perovskites. In this sense, Peng et al. [89] have controlled the selective dissolution of Sr inside the structure La_{0.5}Sr_{0.5}CoO₃ by treating the catalyst with HNO₃. The migration of Sr promotes the NO oxidation and NO_x storage capacities. On the other hand, other authors analyzed the effect of partial substitution of B cation by Pt or Pd [70,92]. The incorporation of these noble metals over perovskite surface has been also explored [92,93]. In both cases the promotion of NO_x adsorption capacity is assigned to generation of structural defects and especially to promotion of NO_x adsorption sites regeneration during the short-rich period.

One of the main drawbacks of bulk perovskites is the crystal growth of the oxide due to the calcination at high temperature during the synthesis. As a result, bulk perovskites usually possess low specific surface areas (usually below 25 m² g⁻¹) and limited NO_x storage sites accessibility [72,76]. Both factors limit NO_x adsorption capacity during lean conditions. Two potential solutions were explored to overcome this limitation: synthesis of mesostructured perovskites via nanocasting method and synthesis of supported perovskite by their distribution over high-surface area materials [94].

Regarding supported perovskites, He et al. [94] found that the distribution of 20 wt % of LaCoO₃ perovskite over ZrTiO₄ support limited sintering of perovskite. As consequence of the higher accessibility of the perovskite the NO_x storage capacity was promoted. In fact, the perovskite-based catalyst exhibited higher NSC than Pt-based catalysts due to the promoted NO-to-NO₂ oxidation behavior. Alternatively, You et al. [95,96] observed that the impregnation of a 10 wt % of LaCoO₃ perovskite over ceria and Ce_{0.75}Zr_{0.25}O₂ supports provides high NO_x storage and reduction capacity. More conventional supports with lower price and higher surface area have been also explored. Ding et al. [97] confined the La_{0.7}Sr_{0.3}CoO₃ perovskite nanoparticles (60 wt %) on mesoporous silica. This sample significantly increased the NO_x adsorption capacity per sample mass unit at 300 °C with respect to bulk sample. Recently, we have prepared alumina-supported perovskites (10–50 wt % La_{0.7}Sr_{0.3}CoO₃/Al₂O₃) by the impregnation of the La_{0.7}Sr_{0.3}CoO₃ over γ-Al₂O₃ [87]. As observed in Figure 4, the distribution of the bulk perovskite over alumina support inhibited the agglomeration of the former. The higher distribution of perovskite phase favors the diffusion of intermediate compounds from oxidation to NO_x adsorption sites. The intermediate loading (30 wt % La_{0.7}Sr_{0.3}CoO₃/Al₂O₃) maximized the efficient use of perovskite phase. This fact was as a consequence of a best balance between well-developed perovskite phase and NO oxidation as well as NO adsorption sites (oxygen vacancies, structural La and Sr at the surface, and segregated SrCO₃) distribution. In fact, the NO_x storage capacity normalized per perovskite mass unit ($NSC = 305.8 \mu\text{mol NO}_x (\text{g}_{\text{LSCO}})^{-1}$) was three times higher than that of bulk perovskite ($NSC = 115.0 \mu\text{mol NO}_x (\text{g}_{\text{LSCO}})^{-1}$).

Regarding perovskites with ordered structures, the studies are scarce and the preparation methods are more complex. Ye et al. [65] compared the catalytic behavior of LaCoO₃ bulk perovskite and a mesoporous-ordered LaCoO₃ perovskite prepared by nanocasting. The latter was obtained by nanocasting using SBA-15 silica as hard-template. As can be observed in Figure 5, the agglomeration of perovskite is significantly inhibited for the sample prepared by nanocasting. As a result, the NSC increases from 93 μmol NO_x g⁻¹ for the sample prepared by conventional method to 252 μmol NO_x g⁻¹ for the sample prepared by nanocasting. The higher NSC can be attributed to the following aspects: (1) more active sites are exposed due to its much larger specific surface area; (2) easier transportation of reactants and products during reactions due to the mesoporous structure; (3) larger number of oxygen vacancies; (4) presence of high-valence cobalt ions (Co^{3+δ}). Alternatively, the conformation of La_{0.8}Cs_{0.2}Mn_{0.8}Ga_{0.2}O₃ perovskites with cotton-like morphology consisting of nanoparticles and nanorods [98] or ZnO nanorod array supported Pt:La_{0.8}Sr_{0.2}MnO₃ lean NO_x traps [99], emerge as more complex alternatives of improvement of the storage capacity of NO_x. Recently, Alcalde-Santiago et al. [100] prepared macroporous SrTi_{1-x}Cu_xO₃ perovskites with high NO_x adsorption capacities.

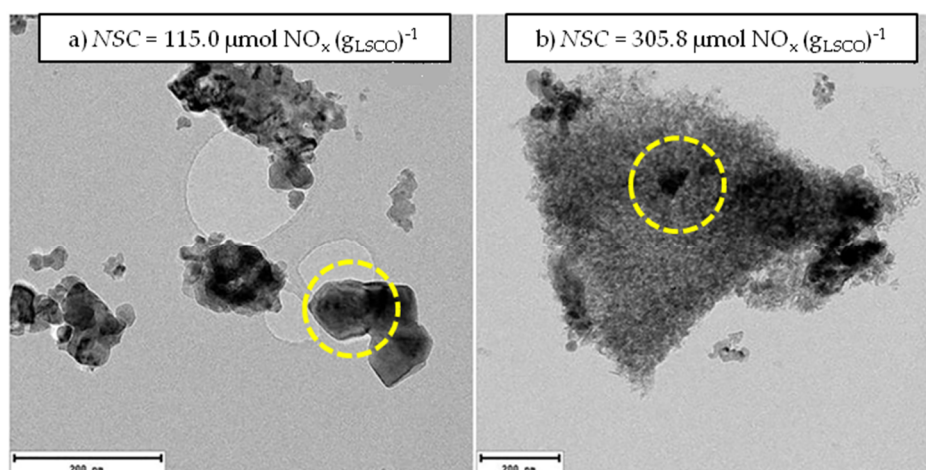


Figure 4. TEM images and NO_x storage capacities (NSC) at $400\text{ }^\circ\text{C}$ normalized per gram of perovskite of: (a) $\text{La}_{0.7}\text{Sr}_{0.3}\text{CoO}_3$ and (b) 30 wt % $\text{La}_{0.7}\text{Sr}_{0.3}\text{CoO}_3/\text{Al}_2\text{O}_3$ samples. Adapted from ref. [87]. Copyright (2018) Elsevier.

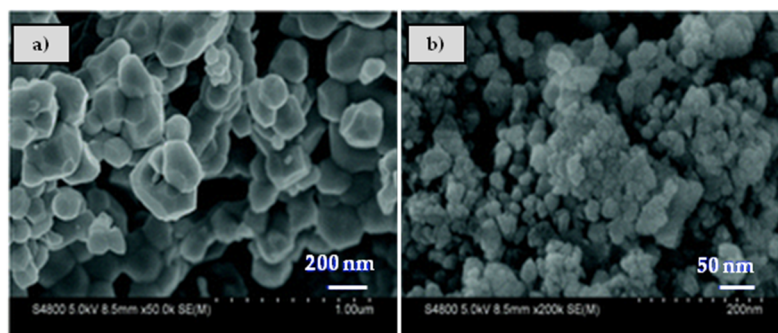


Figure 5. SEM images for LaCoO_3 perovskite prepared by (a) conventional method and (b) nanocasting, respectively. Adapted from [65]. Copyright (2013) Royal Society of Chemistry.

As previously reported, NSR catalysts usually contain strong basic components to promote the trapping of the acidic NO_x molecules. This fact motivated the incorporation of small amounts of basic components over perovskite-based formulation, or alternatively, the mixing of the perovskite with a phase with high NO_x trapping efficiency. Ye et al. [65] observed that the incorporation of K (5 wt % of K_2CO_3) into the mesostructured LaCoO_3 perovskite increased the adsorption capacity from $252\text{ }\mu\text{mol NO}_x\text{ g}^{-1}$ to $981\text{ }\mu\text{mol NO}_x\text{ g}^{-1}$ at $350\text{ }^\circ\text{C}$, due to the presence of a higher concentration of surface basic sites. On the other hand, Qi et al. [72,76] in their studies ball-milled LaMnO_3 perovskite with $\text{Ba}/\text{Al}_2\text{O}_3$ catalyst to promote NO_x adsorption efficiency during the lean period. Alternatively, Wen et al. [101] loaded LaCoO_3 perovskite (25 wt %) on Al_2O_3 support by mechanical mixing. Subsequently, K_2CO_3 (16 wt %) and Pt (0, 0.3, and 1 wt %) were loaded on $\text{LaCoO}_3/\text{Al}_2\text{O}_3$ by the conventional impregnation method. Meanwhile, You et al. [95,96] incorporated increasing contents of K_2CO_3 ($x = 1\text{--}8$ wt %) on $\text{LaCoO}_3/\text{CeO}_2$ and $\text{LaCoO}_3/\text{Ce}_{0.75}\text{Zr}_{0.25}\text{O}_2$ catalysts. In this case, NO_x storage capacity was maximized for the samples with 3–5 wt % of K_2CO_3 due to the presence of higher concentration of homogeneously distributed NO_x adsorption sites at the surface. This activates a new NO_x storage pathway in form of nitrates and/or nitrites formed due to the reaction between K_2CO_3 and NO_x .

3.3. NO_x Reduction

Perovskites have demonstrated as promising materials for NO oxidation and NO_x storage in an oxygen-rich atmosphere. However, the final aim of NSR system is to reduce efficiently the NO_x stored during the lean period preferentially to N_2 in the subsequent short-rich period. Thus, perovskites

should also be good NO_x reduction catalysts in a fuel-rich atmosphere. In this sense, few works analyze the NO_x removal efficiency of perovskite-based formulations. Table 3 summarizes the most relevant results found in the scientific literature related to the utilization of perovskite-based formulations as NSR catalyst.

Table 3. DeNO_x activity of different perovskite-based formulations

Formulation	Feedstream (lean/rich)	GHSV, h ⁻¹	X _{NO_x} , %/S _{N₂} , %	Ref.
5 wt % K/LaCoO ₃ ⁽⁺⁾	[NO] = 400 ppm; [O ₂] = 5%; [C ₃ H ₆] = 1000 ppm (180 s)/[C ₃ H ₆] = 1000 ppm (60 s)	80,000	97.0/97.3	[65]
La _{0.7} Sr _{0.3} CoO ₃	NO] = 500 ppm; [O ₂] = 6.7%; [C ₃ H ₆] = 1000 ppm (180 s)/[NO] = 500 ppm; [C ₃ H ₆] = 1000 ppm (60 s)	80,000	71.4/100	[66]
La _{0.7} Sr _{0.3} Co _{0.97} Pd _{0.03} O ₃	[NO] = 500 ppm; [O ₂] = 6.7% (120 s)/[NO] = 500 ppm; [C ₃ H ₆] = 0.1% (60 s)	32,000	> 90.0/> 90.0	[67]
30 wt % La _{0.7} Sr _{0.3} CoO ₃ /Al ₂ O ₃	[NO] = 500 ppm; [O ₂] = 6%; (150 s)/[NO] = 500 ppm; [H ₂] = 3%; (20 s)	123,500	46.9/53.3	[102]
1.5 wt % Pd–30 wt % La _{0.7} Sr _{0.3} CoO ₃ /Al ₂ O ₃	[NO] = 500 ppm; [O ₂] = 6%; (150 s)/[NO] = 500 ppm; [H ₂] = 3%; (20 s)	123,500	79.2/89.7	[102]
1.4 wt % Pd/La _{0.7} Sr _{0.3} CoO ₃	[NO] = 400 ppm; [O ₂] = 5%; (50 s)/[C ₃ H ₆] = 1000 ppm (10 s) ^(*)	120,000 ^(b)	90.4/n.d.	[92]
La _{0.5} Sr _{0.5} CoO ₃	[NO] = 500 ppm; [O ₂] = 5% (120 s)/[NO] = 500 ppm; [C ₃ H ₆] = 1000 ppm (60 s)	120,000 ^(b)	42.4/n.a.	[89]
LaCo _{0.92} Pt _{0.08} O ₃	[NO] = 280 ppm; [O ₂] = 8% (120 s)/[NO] = 280 ppm; [H ₂] = 3.5% (30 s)	72,000	90.0/70.0 ^(*)	[70]
5 wt % K ₂ CO ₃ –20% LaCoO ₃ /S ^(a)	NO] = 400 ppm; [O ₂] = 5%; (180 s)/[C ₃ H ₆] = 1000 ppm (60 s)	45,000	98.2/98.8	[95]
0.3 wt % Pt–16 wt % K–25 wt % LaCoO ₃ /Al ₂ O ₃	[NO] = 500 ppm; [O ₂] = 8%; (120 s)/[NO] = 500 ppm; [H ₂] = 3.5%; (120 s)	n.a.	~80/90	[101]
LaMnO ₃ + 4 wt % Pd/Al ₂ O ₃ + 2 wt % Rh/CeO ₂ –ZrO ₂ ^(c)	[NO] = 400 ppm; [O ₂] = 10% (60 s)/[NO] = 400 ppm; [H ₂] = 1%; [CO] = 3% (5s)	25,000	85/n.a. ^(*)	[72]
La _{0.9} Sr _{0.1} MnO ₃ + (1.6 wt % Pd + 0.16 wt % Rh)–20 wt % Ba/CeO ₂ –ZrO ₂ ^(c)	[NO] = 200 ppm; [O ₂] = 10% (60 s)/[NO] = 200 ppm; [H ₂] = 1%; [CO] = 3% (5s)	50,000	> 90/n.a. ^(*)	[23]
La _{0.7} Ba _{0.3} Fe _{0.776} Nb _{0.194} Pd _{0.03} O ₃	[NO] = 512 ppm; [O ₂] = 5%; [C ₃ H ₆] = 200 ppm (54 s)/[NO] = 512 ppm; [CO] = 4% (6 s)	n.a.	47/n.a.	[90]

^(*) Presence of H₂O and/or CO₂. ⁽⁺⁾ Prepared by nanocasting. ^(a) S = Ce_{0.75}Zr_{0.25}O₂-doped with 5 wt % Y. ^(b) Units (mL g⁻¹ h⁻¹). ^(c) Monolith.

BaFeO_{3-x} [84] and La_{0.7}Ba_{0.3}Fe_{0.776}Nb_{0.194}Pd_{0.03}O₃ [90] were the alternatives firstly explored; however, these perovskites did not show high NO_x removal efficiency. Kim et al. [23] were the first that observed comparable results to conventional formulations in the application of perovskite-based catalysts as DOC and also as LNT. Specifically, their monolithic catalyst based on La_{0.9}Sr_{0.1}MnO₃ perovskite ball-milled with Pd–Rh/BaO/CeO₂–ZrO₂ catalyst, with noble metal contents (1.8 Pd/0.2 Rh, g L⁻¹) somewhat lower than a commercial catalyst (1.6 Pt/0.3 Pd/0.2 Rh, g L⁻¹), showed a NO_x removal efficiency similar to the commercial catalyst in the presence of CO₂ and H₂O. More recently, two consecutive studies carried out by researchers from General Motors [72,76] analyzed the catalytic behavior and reaction mechanism of a monolithic LaMnO₃ + 4 wt % Pd/Al₂O₃ + 2 wt % Rh/CeO₂–ZrO₂ prepared by ball-milling. Figure 6 shows the NO, NO₂ and ammonia concentration profiles at 35 °C under cycling lean (60 s)/rich (5 s) periods over Pd/Rh/LaMnO₃/BaO/Al₂O₃ catalyst with a SV = 25,000 h⁻¹. The lowest NO_x outlet concentration is observed at the beginning of the lean period due the NO_x adsorption over basic sites (Feed composition: 400 ppm NO, 10% O₂, H₂O, CO₂, and N₂ as balance). As increasing lean period duration, NO_x trapping sites become gradually saturated

and thus NO_x concentration at the reactor outlet increased. In any case, a significant amount of NO_x was adsorbed on the catalyst during the lean period. In fact, a maximum NO outlet concentration of 25 ppm upon switching to rich period was reached after six cycles. This indicates that more than 90% of NO_x are stored. During the short-rich period, oxygen was replaced by a mix of reductant gases (1% H_2 , 3% CO). As a result, the stored NO_x are released as NO with a very small amount of ammonia upon switching to a rich feed. This indicates that the reaction between desorbed NO_x and reductant gases ($\text{CO} + \text{H}_2$) occurred. Indeed, this formulation showed NO_x conversions above 85% and selectivity towards NH_3 around 25%. Taking into account the mechanism of the process, numerous similarities with the Pt-based model catalysts were confirmed. In fact, this formulation showed similar temperature dependence of NO_x storage and reduction to the conventional Pt–Ba/ Al_2O_3 catalyst. However, Constantinou et al. [76] found some differences in their study: (i) a greater resistance to diffusion of nitrates at low temperature, (ii) a faster decomposition of nitrates in reducing environment, and (iii) a greater inhibition of the OSC (oxygen storage capacity) by nitrates.

Alternatively, other studies tried to develop new alternatives based on simpler perovskite-based formulations. In the study carried out by Li et al. [66], the improvement of the NO_x storage capacity for the catalyst $\text{La}_{0.7}\text{Sr}_{0.3}\text{CoO}_3$ after Sr doping was also accompanied by an improvement of the reduction of NO_x with C_3H_6 . This catalyst showed NO_x conversion of 71% and selectivity towards N_2 of 100%. However, the results were obtained with relative high rich/lead periods ratio (60 s/180 s), and continuous admission of the reducing agent (C_3H_6). In order to obtain higher NO_x reduction efficiency, small contents of noble metals, especially Pd, are incorporated on perovskite-based formulation. Two preparation methods were explored for the synthesis of noble metal containing perovskite-based formulations: impregnation or doping the perovskite structure. Li et al. [67] proposed the incorporation of Pd inside the perovskite structure ($\text{La}_{0.7}\text{Sr}_{0.3}\text{Co}_{0.97}\text{Pd}_{0.03}\text{O}_3$) by doping as a simple way to improve the NO_x reduction efficiency of the catalyst. In their study, the Pd accommodation within the lattice was demonstrated by the results obtained by XRD, XPS, and EXAFS experiments. This formulation achieved high NO_x conversions and selectivity towards N_2 above 90%, feeding C_3H_6 (0.1%) only during the rich period. In fact, the NO_x removal efficiency was similar to that observed for conventional NSR formulation, as observed in Figure 7. However, the duration ratio of rich/lead periods remained high (60 s/120 s).

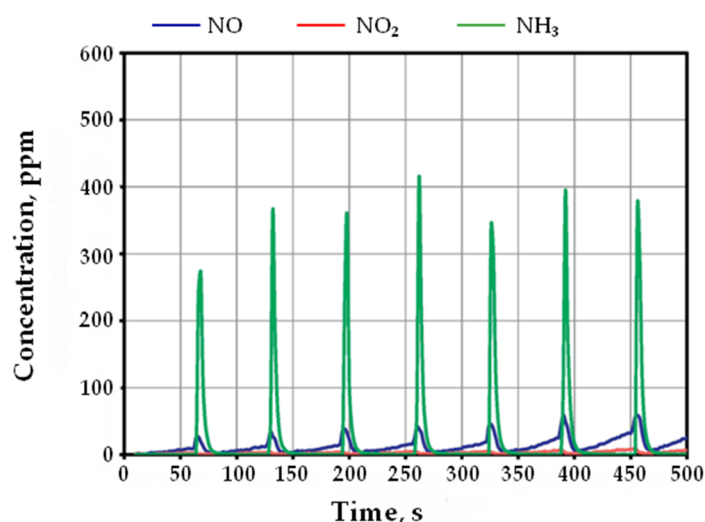


Figure 6. NO (blue), NO_2 (red) and NH_3 (green) concentration profiles at 350 °C under standard LNT test conditions with a GHSV = 25,000 h^{-1} . Catalyst: Pd/Rh/ $\text{LaMnO}_3/\text{BaO}/\text{Al}_2\text{O}_3$ (0 g/L Pt, 1.4 g/L Pd, 0.2 g/L Rh). Reprinted from [72]. Copyright (2012) Elsevier.

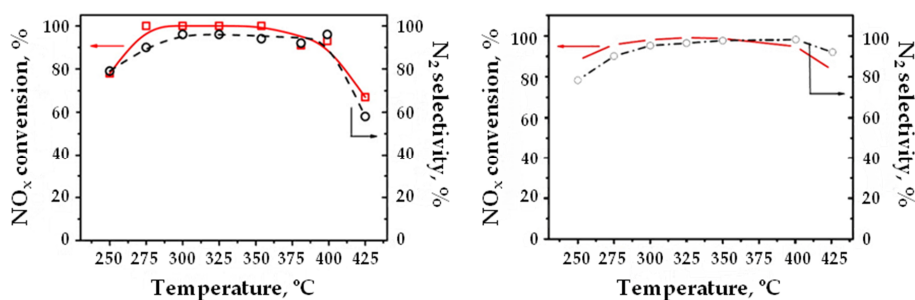


Figure 7. NO_x conversion and N₂ selectivity of the La_{0.7}Sr_{0.3}Co_{0.97}Pd_{0.03}O₃ (left) and 1 wt % Pt–15 wt % Ba/Al₂O₃ samples in the lean/rich cycles as a function of the operating temperatures with a space velocity of 32,000 h⁻¹. Adapted from [67]. Copyright (2013) American Chemical Society.

For the first in the literature, Zhao et al. [92] compared the NO_x removal efficiency of two Pd-based La_{0.7}Sr_{0.3}CoO₃ perovskites prepared by impregnation or doping the perovskite structure. As a general trend, NO_x storage and reduction efficiency is significantly promoted after the incorporation of Pd. The improvement of the NO_x removal efficiency is assigned to a promotion of NO_x adsorption sites regeneration and NO_x reduction rate during rich period (Figure 8). Thus, the higher accessibility of Pd obtained by impregnation method further promoted these steps for Pd-impregnated sample. More recently, we synthesized different catalysts with increasing palladium loadings (0.75, 1.5, 2.25 and 3.0 wt %) incorporated by both methodologies over 30 wt % La_{0.7}Sr_{0.3}CoO₃/Al₂O₃ formulation [102]. As a general trend, Pd-impregnated samples showed higher NO_x-to-N₂ conversion than Pd-doped samples. In agreement with the observed by TEM-EDX mapping and XRD analysis, this fact was ascribed to the partial accommodation of Pd inside the perovskite structure observed for Pd-doped sample, which limits Pd accessibility during lean-rich periods. Among Pd-impregnated samples, the 1.5 wt % Pd–30 wt % La_{0.7}Sr_{0.3}CoO₃/Al₂O₃ variant achieved the best balance between NO_x storage and reduction activity and minimum palladium content. Specifically, their NO_x conversion and nitrogen production were as high as 86% and 70%, respectively. In fact, this formulation achieved comparable DeNO_x activity to the model NSR catalyst (1.5 wt % Pt–15 wt % BaO/Al₂O₃). These results confirm the potential of the 1.5 wt % Pd–30 wt % La_{0.7}Sr_{0.3}CoO₃/Al₂O₃ catalyst for NO_x removal in diesel automobile applications. On the other hand, Wang et al. [70] and Wen et al. [101] analyzed the effect of Pt on NO_x removal efficiency of LaCo_{0.92}Pt_{0.08}O₃ and 0.3 wt % Pt/K₂CO₃/LaCoO₃/Al₂O₃ formulations, respectively. These alternatives showed NO_x-to-N₂ removal efficiencies comparable or superior to 1 wt % Pt–16 wt % Ba/Al₂O₃ catalyst. However, the Pt load in the former was high (~6.0 wt % Pt), whereas the catalyst composition was too complex in the later, which makes them less promising than the previously described.

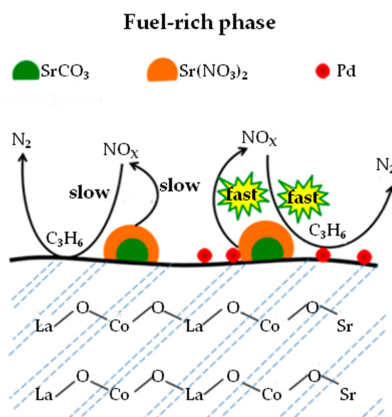


Figure 8. Possible NO_x reduction routes on 1.4 wt % Pd/La_{0.7}Sr_{0.3}CoO₃ perovskite. Reprinted from [92]. Copyright (2018) American Chemical Society.

Taking into account results reported for NO_x storage capacity, the incorporation of perovskites on high surface area supports is presented as an alternative for partial or total replacement of Pt in these formulations. You et al. [95,96] observed how the catalyst 5 wt % K₂CO₃–10 wt % LaCoO₃/S (with S = Ce_{0.75}Zr_{0.25}O₂ doped with 5% Y) provided NO_x reduction efficiencies of 98% and selectivities towards N₂ of 99% at 350 °C. The high activity of these formulations (even in the presence of CO₂ in the feed) is assigned to the high oxidation capacity of NO, and dispersion of the NO_x storage centers (K), which favors a good contact between both phases and the diffusion of intermediate compounds. However, although the results obtained are apparently promising, the reducing periods used in their experiments were too long (60 s) and the space velocities too low (45,000 h⁻¹). In addition, the results were obtained in absence of NO in the rich period. As observed for NO_x adsorption, the conformation of mesoporous perovskites with ordered structure has also been analyzed. The 5 wt % K₂CO₃/LaCoO₃ formulation prepared by nanocasting and sequential impregnation of K₂CO₃ showed NO_x reduction efficiencies of 97% and N₂ selectivities of 97% at 350 °C [65]. However, again the reducing periods used are considered long (60 s), and the results were obtained in absence of NO in the rich period and feeding reducing agent (C₃H₆) in both periods. On the other hand, the ordered macroporous SrTi_{1-x}Cu_xO₃ perovskites showed a limited NO_x reduction capacity and a high influence of CO₂ and H₂O, which limits their actual application [100].

3.4. SO₂ and Hydrothermal Resistance

Based on above described results, perovskite-based formulations can be proposed as an economical alternative to 1.5 wt % Pt–15 wt % BaO/Al₂O₃ model catalyst. However, one of the essential characteristics of the NSR catalyst for application in the exhaust aftertreatment of diesel engines is the durability, basically referring to hydrothermal resistance. In this sense, Pt-based model catalyst shows poor hydrothermal stability and limited sulfur resistance [103,104]. Thus, to comply the characteristics required for real application, the perovskite-based formulations should show high NO_x removal efficiency with simple and complex feedstreams, appropriate hydrothermal stability, and sulfur resistance. In order to have a more realistic vision on these aspects, some of the works previously reported also analyzed the hydrothermal and sulfur resistance of the corresponding perovskite-based formulations.

Regarding sulfur resistance, it is widely accepted that the decrease of NO_x removal efficiency after sulfur poisoning is derived from a significant decrease of NO_x adsorption capacity during lean period. This fact is assigned to the formation of very stable sulfates over basic components of the NSR catalyst. Kim et al. [23] observed that their monolithic catalyst based on La_{0.9}Sr_{0.1}MnO₃ perovskite ball-milled with Pd–Rh/BaO/CeO₂–ZrO₂ catalyst showed higher sulfur resistance and regenerability after SO₂ poisoning. More recently a new concept has emerged based on the results reported by Nishihata et al. [105]. In that work, the authors observed for Pd-doped perovskites a self-regeneration of Pd⁰/Pd²⁺ in and out of perovskite lattices when switching between oxidizing and reducing atmospheres. This behavior could improve the hydrothermal and sulfur resistance of perovskite-based materials. Taking these results as reference, Li et al. [67] also explored the sulfur resistance of La_{0.7}Sr_{0.3}Co_{0.97}Pd_{0.03}O₃ perovskite. This formulation shows excellent sulfur tolerance. Based on the results obtained by EXAFS, XPS, and XRD analysis, this behavior was related to the Pd mobility in the perovskite structure, as outlined in Figure 9. In contrast, the Pt–BaO/Al₂O₃ catalyst was readily poisoned by sulfur (NO_x conversion dropping from 99% to 55%, N₂ selectivity dropping from 96% to 85%) and could not recover its initially catalytic activity by reducing in H₂ at mild temperatures, such as 325 °C. Apparently, the Pd-doped perovskite provides a new possibility for overcoming the problems caused by sulfur poisoning for the LNT systems.

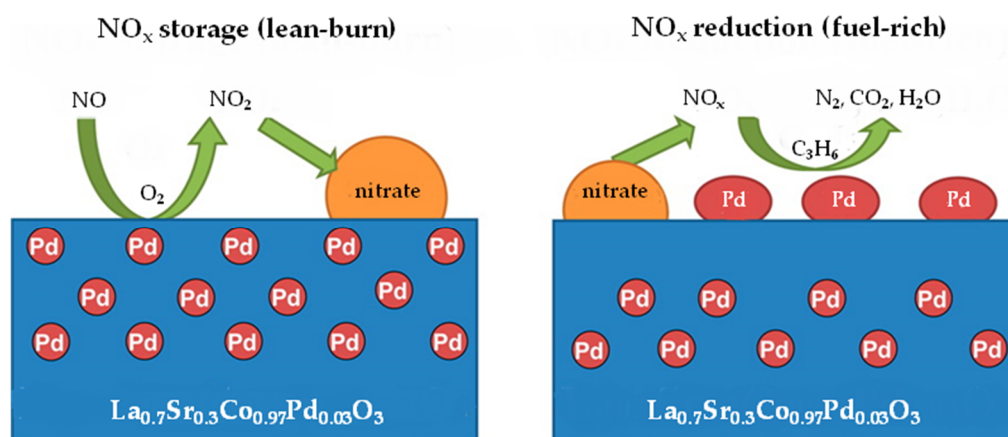


Figure 9. NO_x storage and reduction routes and Pd mobility scheme on for La_{0.7}Sr_{0.3}Co_{0.97}Pd_{0.03}O₃ perovskite during alternative lean-rich cycles. Reprinted from [67]. Copyright (2013) American Chemical Society.

More recently, Wang et al. [70] compared the sulfur resistance of LaCo_{0.92}Pt_{0.08}O₃ and 1 wt % Pt–16 wt % Ba/Al₂O₃ catalysts. As observed in Figure 10, both formulations are quickly deactivated in the presence of 100 ppm of SO₂, but LaCo_{0.92}Pt_{0.08}O₃ shows higher regeneration ability than Pt–Ba/Al₂O₃ in the lean period. This fact is assigned to the formation of surface and bulk cobalt sulfate on LaCo_{0.92}Pt_{0.08}O₃ perovskite, which is less stable than bulk barium sulfate under reducing conditions. The sulfur resistance of LaCoO₃ perovskites was also highlighted in the simultaneous removal of NO_x and soot [106].

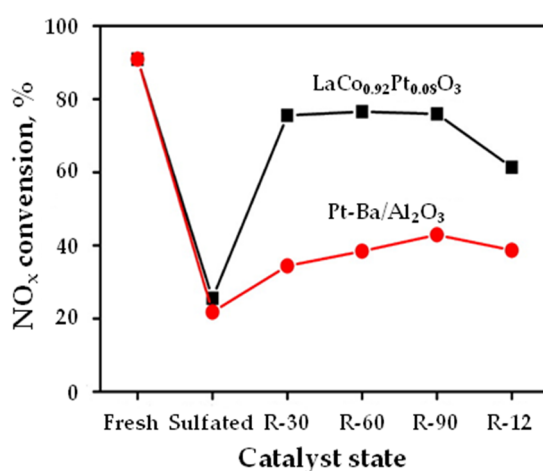


Figure 10. NO_x conversion of LaCo_{0.92}Pt_{0.08}O₃ and 1 wt % Pt–16 wt % Ba/Al₂O₃ at 350 °C for fresh, sulfated, and regenerated (R) catalysts. Reprinted from [70]. Copyright (2013) American Chemical Society.

Regarding hydrothermal resistance, the limited stability of the NSR model formulation is ascribed to Pt progressive agglomeration during reactions as well as the formation of BaAl₂O₄ phase. Wang et al. [70] compared the thermal stability of LaCo_{0.92}Pt_{0.08}O₃ and model NSR catalyst (Pt–Ba/Al₂O₃). For that, samples were first treated in a muffle at 850 °C for 40 h and then submitted to stability test. As shown in the left side of the Figure 11, LaCo_{0.92}Pt_{0.08}O₃ has a much better thermal stability than conventional Pt–Ba/Al₂O₃. As observed in Figure 11, the particle size of Pt–Ba/Al₂O₃ catalyst increased from 4–6 nm to 26–46 nm after hydrothermal aging. In contrast, fine Pt particles (about 4–7 nm) accommodated in the perovskite structure have no obvious change after LaCo_{0.92}Pt_{0.08}O₃ was thermally aged under the same conditions. Thus, Pt particles sintering at high operating temperature

explains the lower stability of Pt–Ba/Al₂O₃ catalyst. However, good redox property of LaCo_{0.92}Pt_{0.08}O₃ can well maintain its perovskite-type structure. Thus, the self-regeneration of noble metal particles in and out of perovskite lattices when switching between oxidizing and reducing atmospheres seems to prevent it from agglomeration during reactions. On the other hand, as the real feed stream usually contains H₂O, the NO_x removal activity was also compared incorporating a 10% of H₂O in the feed stream (right side of Figure 11). The presence of H₂O results in a quick decrement of NO_x conversion for both formulations. However, the NO_x conversion is rapidly restored after cutting off the supply of water. More recently, Wen et al. [101] also analyzed the hydrothermal and sulfur resistance of 0.3 wt % Pt/K₂CO₃/LaCoO₃ catalyst. This alternative showed NO_x-to-N₂ reduction efficiency, resistance to poisoning with SO₂, regenerability, and durability comparable or superior to Pt–Ba/Al₂O₃ model catalyst.

The results analyzed suggest that the segregated metallic Pd/Pt from perovskite in fuel-rich atmospheres plays a significant role in obtaining promising achievements in reducing deactivation. This provides a new possibility for the application of perovskite-based formulations as alternative to NSR model catalyst and for solving the problems caused by simultaneous sulfur poisoning and noble metal aggregation at high temperatures.

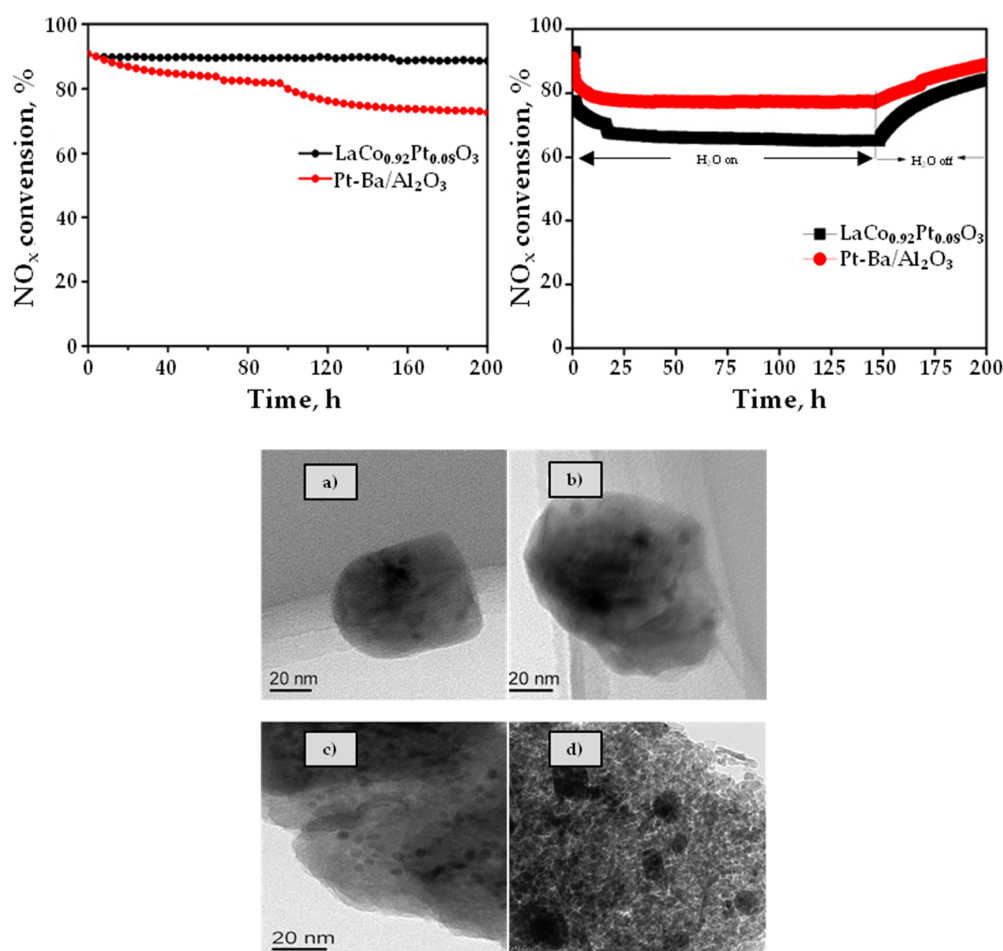


Figure 11. Thermal stability (left) and stability tests with 10 vol% H₂O (right) at 350 °C of LaCo_{0.92}Pt_{0.08}O₃ and Pt–Ba/Al₂O₃. TEM images for (a) LaCo_{0.92}Pt_{0.08}O₃, (c) Pt–Ba/Al₂O₃, (b) aged LaCo_{0.92}Pt_{0.08}O₃, and (d) aged Pt–Ba/Al₂O₃, which were maintained at 850 °C for 40 h followed by NO_x conversion test at 350 °C for 200 h. Reprinted from [70]. Copyright (2013) American Chemical Society.

4. Perovskite-Based Catalysts for Combined NSR–SCR Technology

Results above reported demonstrate that perovskite-based formulations are able to obtain NO_x removal efficiency, hydrothermal stability, and sulfur resistance similar or even higher than conventional NSR model catalyst ($\text{Pt–BaO/Al}_2\text{O}_3$). However, as above mentioned, single-SCR and NSR technologies have some drawbacks that limit their global application in diesel vehicles. These limitations have been partially solved by the implantation of hybrid NSR–SCR, discovered by the Ford Motor company [107]. Since its discovery hybrid NSR–SCR systems have been subjected to a continuous development. Indeed, different system architectures, catalytic formulations and operation control have been analyzed [108–111]. However, the NSR formulation in the combined NSR–SCR configuration is usually based on the Pt-model formulation. As a result, the cost of the hybrid NSR–SCR system increases, whereas its hydrothermal stability decreases. Taking into account the results above reported, the application of perovskite-based formulations in combined NSR–SCR systems can be considered as an improvement of the conventional NSR–SCR configuration.

In a preliminary study, we analyzed the applicability of perovskite-based materials to hybrid NSR–SCR configuration [112]. Figure 12 shows how evolved NO_x ($\text{NO} + \text{NO}_2$), and NH_3 outlet concentration profiles during two consecutive lean-rich periods, as well as mass spectroscopy N_2 signal for the single-NSR and combined NSR–SCR configurations at 300 °C. NSR catalyst correspond to 0.5 wt % Pd–30 wt % $\text{La}_{0.5}\text{Ba}_{0.5}\text{CoO}_3/\text{Al}_2\text{O}_3$ formulation, whereas SCR system is composed of conventional 4% Cu/SAPO-34 formulation. As can be observed in Figure 12a, the single-NSR system shows the typical NO_x outlet concentration profile previously described in Figure 6 [8]. However, when SCR system is placed downstream the NO_x (Figure 12a) and NH_3 (Figure 12b) outlet concentrations decrease drastically in comparison to single-NSR system. These results suggest that most NH_3 formed during regeneration of the NSR catalyst is adsorbed over SAPO-34 zeolite and then, in the subsequent lean period, reacts with the NO_x slipping NSR system following SCR reactions [113]. The occurrence of SCR reactions over the Cu/SAPO-34 catalyst is confirmed by the evolution of N_2 signal measured by MS (Figure 12c). As can be observed, N_2 signal is detected in the rich and lean periods when the reaction was carried out with the combined NSR–SCR system, whereas N_2 formation is only detected during the rich period for the single-NSR systems. When the gas mixture is switched to lean conditions, practically all NO_x is trapped on the NSR catalyst, and consequently, is not available to carry out the SCR reactions with the NH_3 stored in the Cu/SAPO-34 downstream. However, as the NSR catalyst becomes saturated, the gradual increase of NO_x leaving the NSR system promotes the N_2 production by the reduction of non-adsorbed NO_x with the NH_3 previously stored over the acid sites of the zeolite [114]. This fact explains the similar evolution of the NO_x concentration and N_2 signal at the outlet of the combined NSR–SCR system.

In summary, the applicability of 0.5 wt % Pd–30 wt % $\text{La}_{0.5}\text{Ba}_{0.5}\text{CoO}_3/\text{Al}_2\text{O}_3$ catalyst to mixed NSR–SCR system is confirmed. Based on the reported results, the implementation of these types of perovskite-based materials in coupled NSR–SCR configurations can be considered as a promising evolution of the conventional NSR–SCR systems. As a result, this opens a new scope in the development of perovskite-based formulation as a new generation of NSR catalyst to overcome NO_x removal environmental issue in diesel and lean-burn gasoline engines.

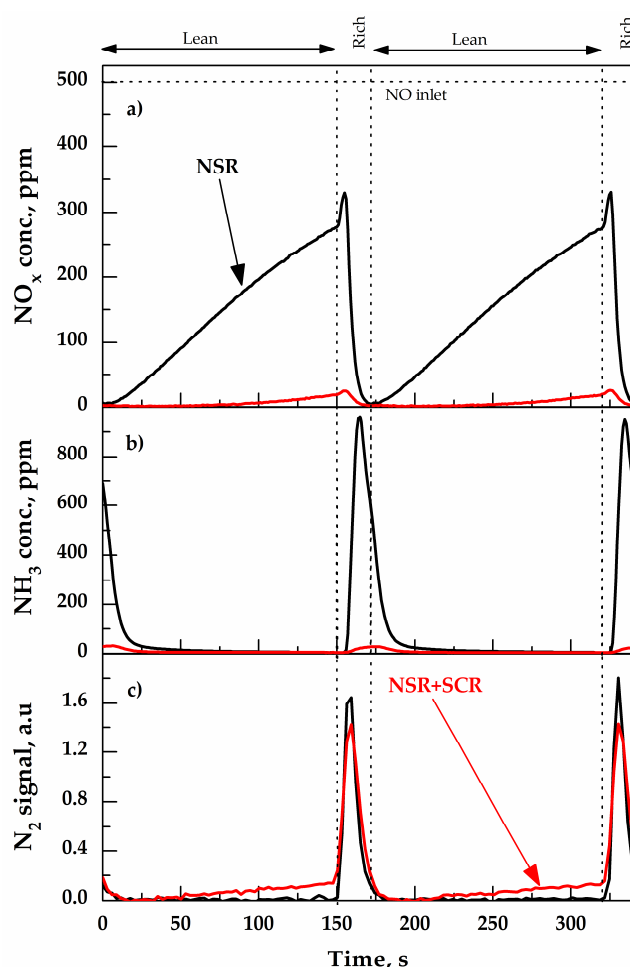


Figure 12. (a) NO_x ($\text{NO} + \text{NO}_2$) and (b) NH_3 outlet concentrations, and (c) MS signal of N_2 for the single-NSR and NSR–SCR configurations at 300 °C. Feed: 500 ppm NO, 6% O_2 /3% H_2 , and Ar to balance; $W/\text{FA}_0 = 200$ (g h mol^{-1}). NSR and SCR formulations correspond to 0.5 wt % Pd–30 wt % $\text{La}_{0.5}\text{Ba}_{0.5}\text{CoO}_3/\text{Al}_2\text{O}_3$ and 4 wt % Cu/SAPO-34 catalysts, respectively [112].

5. Conclusions

Diesel engines offer higher energy efficiency and lower CO_2 emissions than gasoline engines. However, NO_x emission removal diesel engine exhaust gases remains as an unsolved environmental issue. To overcome this technological challenge, two main potential solutions have been developed: NO_x storage and reduction (NSR) and selective catalytic reduction using NH_3 (NH_3 -SCR). However, these technological alternatives show some limitations for extensive application. NSR system shows some NO non-converted as well as large quantities of NH_3 generated during the rich period as byproduct. Furthermore, the catalyst needs large quantities of expensive Pt to obtain high NO_x removal efficiencies. This fact also limits the thermal stability of the system. Otherwise, NH_3 -SCR system requires the urea feeding system for the ammonia injection as chemical reductant. This additional system increases the cost and limits its implementation to light-duty vehicles. Moreover, the limited NO conversion at low temperature and NH_3 slip are some of main of limitations. Recently, combined NSR–SCR configurations have been explored to overtake individual limitations of the stand-alone NSR or SCR systems. In fact, the developed hybrid NSR–SCR systems are able to increase the temperature operational window and NO conversion, and avoid the need for a urea dosing system. Nevertheless, the conventional Pt–Ba/ Al_2O_3 NSR catalyst is the most adopted formulation in coupled NSR–SCR configurations. Thus, a new generation of catalysts and an evolution of the current technologies are essential to reduce NO_x emissions below EURO VI standards.

Perovskite-type oxides can adopt a great range of stoichiometries and crystal structures maintaining a high thermal stability. Indeed, the physico-chemical properties can be controlled by the modification of their composition substituting partially A and B cations. This allows qualify them for their automotive application. As a consequence, perovskite-based materials have been extensively explored as economical and more durable alternative to Pt-based model catalyst for NSR system. La-based formulations, especially LaCoO₃ and LaMnO₃ perovskites, have been the most explored alternative due to their excellent efficiency in NO-to-NO₂ conversion, which is considered a primary step in the NSR process. La³⁺ partial substitution by other cations, such as Ca²⁺, Ba²⁺, or Sr²⁺, is widely accepted as a simple way to improve NO oxidation conversion and NO storage capacity during lean period. The improvement of the NO oxidation activity is closely related to a higher oxygen vacancy density at the surface, which promotes the active oxygen mobility. Meanwhile, the promotion of NO_x storage capacity is ascribed to the promotion of NO-to-NO₂ conversion together with the presence of higher concentration of NO_x adsorption sites at the surface. Unfortunately, bulk perovskites are not efficient enough as NO_x storage and reduction catalyst due to their crystallization at high temperature. Supporting perovskite over high surface area materials, such as Al₂O₃, CeO₂, Ce_{0.75}Zr_{0.25}O₂, SiO₂, or ZrTiO₄, has demonstrated to be an efficient approach. Alternatively, the incorporation of small amounts of basic components, such as Sr, Ba, or K, over perovskite-based formulation, or alternatively, the mixing of the perovskite with a phase with high NO_x trapping efficiency also improves NO_x storage and reduction efficiency. Nonetheless, perovskite-based materials show limited NO_x reduction at low and intermediate temperatures. The incorporation of noble metal (Pt or Pd) low contents by impregnation over perovskite-based formulation or doping perovskite structure emerge as efficient solutions. The former seems to be more appropriate to maximize NO_x removal efficiency. Meanwhile, the latter partially inhibits the agglomeration of noble metal during reactions and promotes sulfur resistance. This fact is ascribed to the self-regeneration of noble metal particles in and out of perovskite lattices during lean-rich cycles. Indeed, these formulations show similar or even higher NO_x removal efficiencies, and hydrothermal and sulfur resistance than conventional Pt–BaO/Al₂O₃ catalyst.

The promising results discussed in the application of perovskite-based formulations to stand-alone NSR system motivated their implementation in hybrid NSR–SCR configurations. The preliminary results have shown almost complete NO_x conversion to N₂ without NH₃ slip. These results are even more promising considering that the noble metal content in the NSR catalyst is significantly lower than in conventional NSR–SCR configuration.

The results reported in this review reveal that perovskites-based materials have emerged as a new generation of material for diesel automotive applications. In upcoming years, more comprehensive studies focused on understanding the mechanism involved in NO_x storage and reduction over perovskite-based formulation, are required. Furthermore, the efficiency of the system during cyclic lean-rich periods can be further promoted. It is worth to mention that the application of perovskite composed materials to the combined NSR–SCR system is very recent. Thus, this opens a new horizon on diesel engines aftertreatment systems with ample room for improvement. Efforts should be focused on exploring different catalyst architectures (i.e., segmented zones or dual layer monoliths), reducing the cost of the catalyst and developing of detailed kinetic model.

Author Contributions: J.A.O.-C. prepared the original draft of the manuscript, B.P.-A. and J.R.G.-V. equally contributed to the writing, review and editing. All authors have read and agreed to the published version of the manuscript.

Funding: Support from the Spanish Ministry of Economy and Competiveness (Project CTQ2015–67597–C2–1–R), the Basque Government (IT1297–19), and the University of the Basque Country acknowledged. One of the authors (JAOC) was supported by a PhD research fellowship provided by the Basque Government (PRE_2014_1_396).

Conflicts of Interest: The authors declare no conflict of interest.

References

1. Srinivasacharya Ayodhya, A.; Gottkere Narayanappa, K. An overview of after-treatment systems for diesel engines. *Environ. Sci. Pollut. Res.* **2018**, *25*, 35034–35047. [[CrossRef](#)]
2. Johnson, T. Review of diesel emissions and control. *Int. J. Engine Res.* **2009**, *10*, 275–285. [[CrossRef](#)]
3. Granger, P.; Parvulescu, V.I. Catalytic NO_x Abatement Systems for Mobile Sources: From Three-Way to Lean Burn after-Treatment Technologies. *Chem. Rev.* **2011**, *111*, 3155–3207. [[CrossRef](#)] [[PubMed](#)]
4. Tronconi, E.; Nova, I. *Urea-SCR Technology for deNO_x after Treatment of Diesel Exhausts*; Springer: New York, NY, USA, 2014.
5. González-Velasco, J.R.; Pereda-Ayo, B.; De-La-Torre, U.; Urrutxua, M.; López-Fonseca, R. Coupled NSR-SCR Systems for NO_x Removal in Light-Duty Vehicles. *ChemCatChem* **2018**, *10*, 2928. [[CrossRef](#)]
6. Takahashi, N.; Shinjoh, H.; Iijima, T.; Suzuki, T.; Yamazaki, K.; Yokota, K.; Suzuki, H.; Miyoshi, N.; Matsumoto, S.; Tanizawa, T.; et al. The new concept 3-way catalyst for automotive lean-burn engine: NO_x storage and reduction catalyst. *Catal. Today* **1996**, *27*, 63–69. [[CrossRef](#)]
7. Clayton, R.D.; Harold, M.P.; Balakotaiah, V. Performance features of Pt/BaO lean NO_x trap with hydrogen as reductant. *AIChE J.* **2009**, *55*, 687–700. [[CrossRef](#)]
8. Pereda-Ayo, B.; Duraiswami, D.; Delgado, J.J.; López-Fonseca, R.; Calvino, J.J.; Bernal, S.; González-Velasco, J.R. Tuning operational conditions for efficient NO_x storage and reduction over a Pt–Ba/Al₂O₃ monolith catalyst. *Appl. Catal. B Environ.* **2010**, *96*, 329–337. [[CrossRef](#)]
9. Pihl, J.; Parks, J.; Daw, C.; Root, T. Product Selectivity During Regeneration of Lean NO_x Trap Catalysts. *SAE Tech. Pap.* **2006**. [[CrossRef](#)]
10. Pereda-Ayo, B.; López-Fonseca, R.; González-Velasco, J.R. Influence of the preparation procedure of NSR monolithic catalysts on the Pt–Ba dispersion and distribution. *Appl. Catal. A Gen.* **2009**, *363*, 73–80. [[CrossRef](#)]
11. Pereda-Ayo, B.; Divakar, D.; López-Fonseca, R.; González-Velasco, J.R. Influence of platinum and barium precursors on the NSR behavior of Pt–Ba/Al₂O₃ monoliths for lean-burn engines. *Catal. Today* **2009**, *147*, S244–S249. [[CrossRef](#)]
12. Colombo, M.; Nova, I.; Tronconi, E. A comparative study of the NH₃-SCR reactions over a Cu-zeolite and a Fe-zeolite catalyst. *Catal. Today* **2010**, *151*, 223–230. [[CrossRef](#)]
13. Ruggeri, M.P.; Selleri, T.; Colombo, M.; Nova, I.; Tronconi, E. Identification of nitrites/HONO as primary products of NO oxidation over Fe-ZSM-5 and their role in the Standard SCR mechanism: A chemical trapping study. *J. Catal.* **2014**, *311*, 266–270. [[CrossRef](#)]
14. De-La-Torre, U.; Pereda-Ayo, B.; Moliner, M.; González-Velasco, J.R.; Corma, A. Cu-zeolite catalysts for NO_x removal by selective catalytic reduction with NH₃ and coupled to NO storage/reduction monolith in diesel engine exhaust aftertreatment systems. *Appl. Catal. B Environ.* **2016**, *187*, 419–427. [[CrossRef](#)]
15. De-La-Torre, U.; Pereda-Ayo, B.; Gutiérrez-Ortiz, M.A.; González-Marcos, J.A.; González-Velasco, J.R. Steady-state NH₃-SCR global model and kinetic parameter estimation for NO_x removal in diesel engine exhaust aftertreatment with Cu/chabazite. *Catal. Today* **2017**, *296*, 95–104. [[CrossRef](#)]
16. Urrutxua, M.; Pereda-Ayo, B.; De La Torre, U.; González-Velasco, J.R. Evaluation of Cu/SAPO-34 Catalysts Prepared by Solid-State and Liquid Ion-Exchange Methods for NO_x Removal by NH₃-SCR. *ACS Omega* **2019**, *4*, 14699–14713. [[CrossRef](#)] [[PubMed](#)]
17. González-Velasco, J.R.; López-Fonseca, R.; Pereda-Ayo, B. NSR Technology. In *NO_x Trap Catalysts and Technologies: Fundamentals and Industrial Applications*; The Royal Society of Chemistry: London, UK, 2018; pp. 36–66.
18. Royer, S.; Duprez, D.; Can, F.; Courtois, X.; Batiot-Dupeyrat, C.; Laassiri, S.; Alamdari, H. Perovskites as Substitutes of Noble Metals for Heterogeneous Catalysis: Dream or Reality. *Chem. Rev.* **2014**, *114*, 10292–10368. [[CrossRef](#)]
19. Libby, W.F. Promising Catalyst for Auto Exhaust. *Science* **1971**, *171*, 499. [[CrossRef](#)]
20. Voorhoeve, R.J.H.; Reimeika, J.P.; Trimble, L.E. Defect Chemistry and Catalysis in Oxidation and Reduction over Perovskite-Type Oxides. *Ann. N. Y. Acad. Sci.* **2006**, *272*, 3–21. [[CrossRef](#)]
21. Zhu, H.; Zhang, P.; Dai, S. Recent Advances of Lanthanum-Based Perovskite Oxides for Catalysis. *ACS Catal.* **2015**, *5*, 6370–6385. [[CrossRef](#)]
22. Zhu, J.; Li, H.; Zhong, L.; Xiao, S.; Xu, X.; Yang, X.; Zhao, Z.; Li, J. Perovskite Oxides: Preparation, Characterizations, and Applications in Heterogeneous Catalysis. *ACS Catal.* **2014**, *4*, 2917–2940. [[CrossRef](#)]

23. Kim, C.H.; Qi, G.; Dahlberg, K.; Li, W. Strontium-doped perovskites rival platinum catalysts for treating NO_x in simulated diesel exhaust. *Science* **2010**, *327*, 1624–1627. [[CrossRef](#)] [[PubMed](#)]
24. Gallagher, P.K.; Johnson, D.W.; Schrey, F. Studies of some supported perovskite oxidation catalysts. *Mater. Res. Bull.* **1974**, *9*, 1345–1352. [[CrossRef](#)]
25. Onrubia, J.A.; Pereda-Ayo, B.; De-La-Torre, U.; González-Velasco, J.R. Key factors in Sr-doped LaBO₃ (B = Co or Mn) perovskites for NO oxidation in efficient diesel exhaust purification. *Appl. Catal. B Environ.* **2017**, *213*, 198–210. [[CrossRef](#)]
26. Zhou, C.; Feng, Z.; Zhang, Y.; Hu, L.; Chen, R.; Shan, B.; Yin, H.; Wang, W.G.; Huang, A. Enhanced catalytic activity for NO oxidation over Ba doped LaCoO₃ catalyst. *RSC Adv.* **2015**, *5*, 28054–28059. [[CrossRef](#)]
27. Zhong, S.; Sun, Y.; Xin, H.; Yang, C.; Chen, L.; Li, X. NO oxidation over Ni–Co perovskite catalysts. *Chem. Eng. J.* **2015**, *275*, 351–356. [[CrossRef](#)]
28. Wen, Y.; Zhang, C.; He, H.; Yu, Y.; Teraoka, Y. Catalytic oxidation of nitrogen monoxide over La_{1-x}Ce_xCoO₃ perovskites. *Catal. Today* **2007**, *126*, 400–405. [[CrossRef](#)]
29. Wang, J.; Su, Y.; Wang, X.; Chen, J.; Zhao, Z.; Shen, M. The effect of partial substitution of Co in LaMnO₃ synthesized by sol–gel methods for NO oxidation. *Catal. Commun.* **2012**, *25*, 106–109. [[CrossRef](#)]
30. Hong, Z.; Wang, Z.; Li, X. Catalytic oxidation of nitric oxide (NO) over different catalysts: An overview. *Catal. Sci. Technol.* **2017**, *7*, 3440–3452. [[CrossRef](#)]
31. Zhu, J.; Thomas, A. ChemInform abstract: Perovskite-type mixed oxides as catalytic material for NO removal. *Appl. Catal. B Environ.* **2010**, *41*, 225–233. [[CrossRef](#)]
32. Zhou, C.; Liu, X.; Wu, C.; Wen, Y.; Xue, Y.; Chen, R.; Zhang, Z.; Shan, B.; Yin, H.; Wang, W.G. NO oxidation catalysis on copper doped hexagonal phase LaCoO₃: A combined experimental and theoretical study. *Phys. Chem. Chem. Phys.* **2014**, *16*, 5106–5112. [[CrossRef](#)]
33. Hong, S.; Lee, G. Simultaneous removal of NO and carbon particulates over lanthanoid perovskite-type catalysts. *Catal. Today* **2000**, *63*, 397–404. [[CrossRef](#)]
34. Li, Z.; Meng, M.; Li, Q.; Xie, Y.; Hu, T.; Zhang, J. Fe-substituted nanometric La_{0.9}K_{0.1}Co_{1-x}Fe_xO_{3-δ} perovskite catalysts used for soot combustion, NO_x storage and simultaneous catalytic removal of soot and NO_x. *Chem. Eng. J.* **2010**, *164*, 98–105. [[CrossRef](#)]
35. Liu, J.; Xu, J.; Zhao, Z.; Duan, A.; Jiang, G.; Jing, Y. A novel four-way combining catalysts for simultaneous removal of exhaust pollutants from diesel engine. *J. Environ. Sci.* **2010**, *22*, 1104–1109. [[CrossRef](#)]
36. Teraoka, Y.; Kanada, K.; Kagawa, S. Synthesis of La_{1-x}K_xMnO perovskite-type oxides and their catalytic property for simultaneous removal of NO_x and diesel soot particulates. *Appl. Catal. B Environ.* **2001**, *34*, 73–78. [[CrossRef](#)]
37. Yao, W.; Wang, R.; Yang, X. LaCo_{1-x}Pd_xO₃ Perovskite-Type Oxides: Synthesis, Characterization and Simultaneous Removal of NO_x and Diesel Soot. *Catal. Lett.* **2009**, *130*, 613–621. [[CrossRef](#)]
38. Wang, K.; Qian, L.; Zhang, L.; Liu, H.; Yan, Z. Simultaneous removal of NO_x and soot particulates over La_{0.7}Ag_{0.3}MnO₃ perovskite oxide catalysts. *Catal. Today* **2010**, *158*, 423–426. [[CrossRef](#)]
39. Dhal, G.C.; Dey, S.; Mohan, D.; Prasad, R. Study of Fe, Co, and Mn-based perovskite-type catalysts for the simultaneous control of soot and NO_x from diesel engine exhaust. *Mater. Discov.* **2017**, *10*, 37–42. [[CrossRef](#)]
40. Ivanov, D.V.; Sadovskaya, E.M.; Pinaeva, L.G.; Isupova, L.E. Influence of oxygen mobility on catalytic activity of La–Sr–Mn–O composites in the reaction of high temperature N₂O decomposition. *J. Catal.* **2009**, *267*, 5–13. [[CrossRef](#)]
41. Ivanov, D.V.; Pinaeva, L.G.; Isupova, L.A.; Sadovskaya, E.M.; Prosvirin, I.P.; Gerasimov, E.Y.; Yakovleva, I.S. Effect of surface decoration with LaSrFeO₄ on oxygen mobility and catalytic activity of La_{0.4}Sr_{0.6}FeO_{3-δ} in high-temperature N₂O decomposition, methane combustion and ammonia oxidation. *Appl. Catal. A Gen.* **2013**, *457*, 42–51. [[CrossRef](#)]
42. Gunasekaran, N.; Rajadurai, S.; Carberry, J.J. Catalytic decomposition of nitrous oxide over perovskite type solid oxide solutions and supported noble metal catalysts. *Catal. Lett.* **1995**, *35*, 373–382. [[CrossRef](#)]
43. Alini, S.; Basile, F.; Blasioli, S.; Rinaldi, C.; Vaccari, A. Development of new catalysts for N₂O-decomposition from adipic acid plant. *Appl. Catal. B Environ.* **2007**, *70*, 323–329. [[CrossRef](#)]
44. Pan, K.L.; Yu, S.J.; Yan, S.Y.; Chang, M.B. Direct N₂O decomposition over La₂NiO₄-based perovskite-type oxides. *J. Air Waste Manag. Assoc.* **2014**, *64*, 1260–1269. [[CrossRef](#)] [[PubMed](#)]

45. Wu, Y.; Dujardin, C.; Lancelot, C.; Dacquain, J.P.; Parvulescu, V.I.; Cabié, M.; Henry, C.R.; Neisius, T.; Granger, P. Catalytic abatement of NO and N₂O from nitric acid plants: A novel approach using noble metal-modified perovskites. *J. Catal.* **2015**, *328*, 236–247. [[CrossRef](#)]
46. Sun, K.; Xia, H.; Hensen, E.; van Santen, R.; Li, C. Chemistry of N₂O decomposition on active sites with different nature: Effect of high-temperature treatment of Fe/ZSM-5. *J. Catal.* **2006**, *238*, 186–195. [[CrossRef](#)]
47. Belessi, V.C.; Trikalitis, P.N.; Ladavos, A.K.; Bakas, T.V.; Pomonis, P.J. Structure and catalytic activity of La_{1-x}FeO₃ system (x = 0.00, 0.05, 0.10, 0.15, 0.20, 0.25, 0.35) for the NO+CO reaction. *Appl. Catal. A Gen.* **1999**, *177*, 53–68. [[CrossRef](#)]
48. Belessi, V.C.; Bakas, T.V.; Costa, C.N.; Efstathiou, A.M.; Pomonis, P.J. Synergistic effects of crystal phases and mixed valences in La–Sr–Ce–Fe–O mixed oxidic/perovskitic solids on their catalytic activity for the NO+CO reaction. *Appl. Catal. B Environ.* **2000**, *28*, 13–28. [[CrossRef](#)]
49. Leontiou, A.A.; Ladavos, A.K.; Pomonis, P.J. Catalytic NO reduction with CO on La_{1-x}Sr_x(Fe³⁺/Fe⁴⁺)O_{3±δ} perovskite-type mixed oxides (x = 0.00, 0.15, 0.30, 0.40, 0.60, 0.70, 0.80, and 0.90). *Appl. Catal. A Gen.* **2003**, *241*, 133–141. [[CrossRef](#)]
50. Wang, Y.; Cui, X.; Li, Y.; Shu, Z.; Chen, H.; Shi, J. A simple co-nanocasting method to synthesize high surface area mesoporous LaCoO₃ oxides for CO and NO oxidations. *Micropor Mesopor. Mater.* **2013**, *176*, 8–15. [[CrossRef](#)]
51. Peter, S.D.; Garbowski, E.; Perrichon, V.; Primet, M. NO reduction by CO over alumina-supported perovskites. *Catal. Lett.* **2000**, *70*, 27–33. [[CrossRef](#)]
52. Shen, S.; Weng, H. Comparative Study of Catalytic Reduction of Nitric Oxide with Carbon Monoxide over the La_{1-x}Sr_xBO₃ (B = Mn, Fe, Co, Ni) Catalysts. *Ind. Eng. Chem. Res.* **1998**, *37*, 2654–2661. [[CrossRef](#)]
53. Varma, S.; Wani, B.N.; Gupta, N.M. Redox behavior and catalytic activity of La–Fe–V–O mixed oxides. *Appl. Catal. A Gen.* **2003**, *241*, 341–348. [[CrossRef](#)]
54. Choi, S.O.; Penninger, M.; Kim, C.H.; Schneider, W.F.; Thompson, L.T. Experimental and Computational Investigation of Effect of Sr on NO Oxidation and Oxygen Exchange for La_{1-x}Sr_xCoO₃ Perovskite Catalysts. *ACS Catal.* **2013**, *3*, 2719–2728. [[CrossRef](#)]
55. Idriss, H.; Barteau, M.A. Active sites on oxides: From single crystals to catalysts. *Adv. Catal.* **2000**, *45*, 261–331.
56. Mars, P.; van Krevelen, D.W. Oxidations carried out by means of vanadium oxide catalysts. *Chem. Eng. Sci.* **1954**, *3*, 41–59. [[CrossRef](#)]
57. Dong, Y.; Xian, H.; Lv, J.; Liu, C.; Guo, L.; Meng, M.; Tan, Y.; Tsubaki, N.; Li, X. Influence of synthesis conditions on NO oxidation and NO_x storage performances of La_{0.7}Sr_{0.3}MnO₃ perovskite-type catalyst in lean-burn atmospheres. *Mater. Chem. Phys.* **2014**, *143*, 578–586. [[CrossRef](#)]
58. Chen, J.; Shen, M.; Wang, X.; Wang, J.; Su, Y.; Zhao, Z. Catalytic performance of NO oxidation over LaMeO₃ (Me = Mn, Fe, Co) perovskite prepared by the sol–gel method. *Catal. Commun.* **2013**, *37*, 105–108. [[CrossRef](#)]
59. Chen, J.; Shen, M.; Wang, X.; Qi, G.; Wang, J.; Li, W. The influence of nonstoichiometry on LaMnO₃ perovskite for catalytic NO oxidation. *Appl. Catal. B Environ.* **2013**, *134–135*, 251–257. [[CrossRef](#)]
60. Białobok, B.; Trawczyński, J.; Miśta, W.; Zawadzki, M. Ethanol combustion over strontium- and cerium-doped LaCoO₃ catalysts. *Appl. Catal. B Environ.* **2007**, *72*, 395–403. [[CrossRef](#)]
61. Dow, W.; Huang, T. Yttria-Stabilized Zirconia Supported Copper Oxide Catalyst: II. Effect of Oxygen Vacancy of Support on Catalytic Activity for CO Oxidation. *J. Catal.* **1996**, *160*, 171–182. [[CrossRef](#)]
62. Islam, M.S.; Cherry, M.; Winch, L.J. Defect chemistry of LaBO₃ (B = Al, Mn or Co) perovskite-type oxides. Relevance to catalytic and transport behavior. *J. Chem. Soc. Faraday Trans.* **1996**, *92*, 479–482. [[CrossRef](#)]
63. Over, H. Surface Chemistry of Ruthenium Dioxide in Heterogeneous Catalysis and Electrocatalysis: From Fundamental to Applied Research. *Chem. Rev.* **2012**, *112*, 3356–3426. [[CrossRef](#)] [[PubMed](#)]
64. Chien, C.; Shi, J.; Huang, T. Effect of Oxygen Vacancy on CO-NO-O₂ Reaction over Yttria-Stabilized Zirconia-Supported Copper Oxide Catalyst. *Ind. Eng. Chem. Res.* **1997**, *36*, 1544–1551. [[CrossRef](#)]
65. Ye, J.; Yu, Y.; Meng, M.; Jiang, Z.; Ding, T.; Zhang, S.; Huang, Y. Highly efficient NO_x purification in alternating lean/rich atmospheres over non-platinic mesoporous perovskite-based catalyst K/LaCoO₃. *Catal. Sci. Technol.* **2013**, *3*, 1915–1918. [[CrossRef](#)]
66. Li, X.G.; Dong, Y.H.; Xian, H.; Hernández, W.Y.; Meng, M.; Zou, H.H.; Ma, A.J.; Zhang, T.Y.; Jiang, Z.; Tsubaki, N.; et al. De-NO_x in alternative lean/rich atmospheres on La_{1-x}Sr_xCoO₃ perovskites. *Energy Environ. Sci.* **2011**, *4*, 3351–3354. [[CrossRef](#)]

67. Li, X.; Chen, C.; Liu, C.; Xian, H.; Guo, L.; Lv, J.; Jiang, Z.; Vernoux, P. Pd-Doped Perovskite: An Effective Catalyst for Removal of NO_x from Lean-Burn Exhausts with High Sulfur Resistance. *ACS Catal.* **2013**, *3*, 1071–1075. [[CrossRef](#)]
68. Ma, A.; Wang, S.; Liu, C.; Xian, H.; Ding, Q.; Guo, L.; Meng, M.; Tan, Y.; Tsubaki, N.; Zhang, J.; et al. Effects of Fe dopants and residual carbonates on the catalytic activities of the perovskite-type La_{0.7}Sr_{0.3}Co_{1-x}Fe_xO₃ NO_x storage catalyst. *Appl. Catal. B Environ.* **2014**, *146*, 24–34. [[CrossRef](#)]
69. Peng, Y.; Si, W.; Li, J.; Crittenden, J.; Hao, J. Experimental and DFT studies on Sr-doped LaMnO₃ catalysts for NO_x storage and reduction. *Catal. Sci. Technol.* **2015**, *5*, 2478–2485. [[CrossRef](#)]
70. Wang, X.; Qi, X.; Chen, Z.; Jiang, L.; Wang, R.; Wei, K. Studies on SO₂ Tolerance and Regeneration over Perovskite-Type LaCo_{1-x}Pt_xO₃ in NO_x Storage and Reduction. *J. Phys. Chem. C* **2014**, *118*, 13743–13751. [[CrossRef](#)]
71. Liu, X.; Chen, Z.; Wen, Y.; Chen, R.; Shan, B. NO oxidation catalysis on copper doped hexagonal phase LaCoO₃: A combined experimental and theoretical study. *Catal. Sci. Technol.* **2014**, *4*, 3687–3696.
72. Qi, G.; Li, W. Pt-free, LaMnO₃ based lean NO_x trap catalysts. *Catal. Today* **2012**, *184*, 72–77. [[CrossRef](#)]
73. Shen, M.; Zhao, Z.; Chen, J.; Su, Y.; Wang, J.; Wang, X. Effects of calcium substitute in LaMnO₃ perovskites for NO catalytic oxidation. *J. Rare Earths* **2013**, *31*, 119–123. [[CrossRef](#)]
74. Yoon, D.Y.; Lim, E.; Kim, Y.J.; Kim, J.H.; Ryu, T.; Lee, S.; Cho, B.K.; Nam, I.; Choung, J.W.; Yoo, S. NO oxidation activity of Ag-doped perovskite catalysts. *J. Catal.* **2014**, *319*, 182–193. [[CrossRef](#)]
75. Albaladejo-Fuentes, V.; López-Suárez, F.; Sánchez-Adsuar, M.S.; Illán-Gómez, M.J. BaTi_{0.8}Cu_{0.2}O₃ Catalysts for NO Oxidation and NO_x Storage: Effect of Synthesis Method. *Appl. Catal. A Gen.* **2017**, *60*, 220–224. [[CrossRef](#)]
76. Constantinou, C.; Li, W.; Qi, G.; Epling, W.S. NO_x storage and reduction over a perovskite-based lean NO_x trap catalyst. *Appl. Catal. B Environ.* **2013**, *134–135*, 66–74. [[CrossRef](#)]
77. Hodjati, S.; Vaezzadeh, K.; Petit, C.; Pitchon, V.; Kiennemann, A. Absorption/desorption of NO_x process on perovskites: Performances to remove NO_x from a lean exhaust gas. *Appl. Catal. B Environ.* **2000**, *26*, 5–16. [[CrossRef](#)]
78. Hodjati, S.; Petit, C.; Pitchon, V.; Kiennemann, A. Absorption/desorption of NO_x process on perovskites: Impact of SO₂ on the storage capacity of BaSnO₃ and strategy to develop thioresistance. *Appl. Catal. B Environ.* **2001**, *30*, 247–257. [[CrossRef](#)]
79. Hodjati, S.; Vaezzadeh, K.; Petit, C.; Pitchon, V.; Kiennemann, A. NO_x sorption–desorption study: Application to diesel and lean-burn exhaust gas (selective NO_x recirculation technique). *Catal. Today* **2000**, *59*, 323–334. [[CrossRef](#)]
80. Milt, V.G.; Querini, C.A.; Miró, E.E.; Ulla, M.A. Abatement of diesel exhaust pollutants: NO_x adsorption on Co,Ba,K/CeO₂ catalysts. *J. Catal.* **2003**, *20*, 424–432. [[CrossRef](#)]
81. Milt, V.G.; Ulla, M.A.; Miró, E.E. NO_x trapping and soot combustion on BaCoO_{3-y} perovskite: LRS and FTIR characterization. *Appl. Catal. B Environ.* **2005**, *57*, 13–21. [[CrossRef](#)]
82. Xian, H.; Zhang, X.; Li, X.; Li, L.; Zou, H.; Meng, M.; Li, Q.; Tan, Y.; Tsubaki, N. BaFeO_{3-x} Perovskite: An Efficient NO_x Absorber with a High Sulfur Tolerance. *J. Phys. Chem. C* **2010**, *114*, 11844–11852. [[CrossRef](#)]
83. Xian, H.; Zhang, X.; Li, X.; Li, L.; Zou, H.; Meng, M.; Zou, Z.; Guo, L.; Tsubaki, N. Effect of the calcination conditions on the NO_x storage behavior of the perovskite BaFeO_{3-x} catalysts. *Catal. Today* **2010**, *158*, 215–219. [[CrossRef](#)]
84. Xian, H.; Li, F.; Li, X.; Zhang, X.; Meng, M.; Zhang, T.; Tsubaki, N. Influence of preparation conditions to structure property, NO_x and SO₂ sorption behavior of the BaFeO_{3-x} perovskite catalyst. *Fuel Process. Technol.* **2011**, *92*, 1718–1724. [[CrossRef](#)]
85. Ge, C.; Li, L.; Xian, H.; Yan, H.; Meng, M.; Li, X. Effects of Ti-doping on the NO_x storage and the sulfur resistance of the BaFe_{1-x}Ti_xO_{3-y} perovskite-type catalysts for lean-burn exhausts. *Fuel Process. Technol.* **2014**, *120*, 1–7. [[CrossRef](#)]
86. Albaladejo-Fuentes, V.; López-Suárez, F.E.; Sánchez-Adsuar, M.S.; Illán-Gómez, M.J. BaTi_{1-x}Cu_xO₃ perovskites: The effect of copper content in the properties and in the NO_x storage capacity. *Appl. Catal. A Gen.* **2014**, *488*, 189–199. [[CrossRef](#)]
87. Onrubia-Calvo, J.A.; Pereda-Ayo, B.; De-La-Torre, U.; González-Velasco, J.R. Strontium doping and impregnation onto alumina improve the NO_x storage and reduction capacity of LaCoO₃ perovskites. *Catal. Today* **2018**, *333*, 208–218. [[CrossRef](#)]

88. Neagu, D.; Tsekouras, G.; Miller, D.N.; Ménard, H.; Irvine, J.T.S. In situ growth of nanoparticles through control of non-stoichiometry. *Nat. Chem.* **2013**, *5*, 916. [[CrossRef](#)]
89. Peng, Y.; Si, W.; Luo, J.; Su, W.; Chang, H.; Li, J.; Hao, J.; Crittenden, J. Surface tuning of $\text{La}_{0.5}\text{Sr}_{0.5}\text{CoO}_3$ perovskite catalysts by acetic acid for NO_x storage and reduction. *Environ. Sci. Technol.* **2016**, *50*, 6442–6448. [[CrossRef](#)]
90. Ueda, A.; Yamada, Y.; Katsuki, M.; Kiyobayashi, T.; Xu, Q.; Kuriyama, N. Perovskite catalyst (La, Ba)(Fe, Nb, Pd) O_3 applicable to NO_x storage and reduction system. *Catal. Commun.* **2009**, *11*, 34–37. [[CrossRef](#)]
91. López-Suárez, F.E.; Illán-Gómez, M.J.; Bueno-López, A.; Anderson, J.A. NO_x storage and reduction on a SrTiCuO_3 perovskite catalyst studied by operando DRIFTS. *Appl. Catal. B Environ.* **2011**, *104*, 261–267. [[CrossRef](#)]
92. Zhao, D.; Gao, Z.; Xian, H.; Xing, L.; Yang, Y.; Tian, Y.; Ding, T.; Jiang, Z.; Zhang, J.; Zheng, L.; et al. Addition of Pd on $\text{La}_{0.7}\text{Sr}_{0.3}\text{CoO}_3$ Perovskite to Enhance Catalytic Removal of NO_x . *Ind. Eng. Chem. Res.* **2018**, *57*, 521–531. [[CrossRef](#)]
93. Say, Z.; Dogac, M.; Vovk, V.I.; Kalay, Y.E.; Kim, C.H.; Li, W.; Ozensoy, E. Palladium doped perovskite-based NO oxidation catalysts: The role of Pd and B-sites for NO_x adsorption behavior via in-situ spectroscopy. *Appl. Catal. B Environ.* **2014**, *154–155*, 51–61. [[CrossRef](#)]
94. He, X.; Meng, M.; He, J.; Zou, Z.; Li, X.; Li, Z.; Jiang, Z. A potential substitution of noble metal Pt by perovskite LaCoO_3 in ZrTiO_4 supported lean-burn NO_x trap catalysts. *Catal. Commun.* **2010**, *10*, 165–168. [[CrossRef](#)]
95. You, R.; Zhang, Y.; Liu, D.; Meng, M.; Zheng, L.; Zhang, J.; Hu, T. YCeZrO Ternary Oxide Solid Solution Supported Nonplatinic Lean-Burn NO_x Trap Catalysts Using LaCoO_3 Perovskite as Active Phase. *J. Phys. Chem. C* **2014**, *118*, 25403–25420. [[CrossRef](#)]
96. You, R.; Zhang, Y.; Liu, F.; Meng, M.; Jiang, Z.; Zhang, S.; Huang, Y. A series of ceria supported lean-burn NO_x trap catalysts $\text{LaCoO}_3/\text{K}_2\text{CO}_3/\text{CeO}_2$ using perovskite as active component. *Chem. Eng. J.* **2015**, *260*, 357–367. [[CrossRef](#)]
97. Ding, Q.; Xian, H.; Tan, Y.; Tsubaki, N.; Li, X. Mesoporous SiO_2 -confined $\text{La}_{0.7}\text{Sr}_{0.3}\text{CoO}_3$ perovskite nanoparticles: An efficient NO_x adsorber for lean-burn exhausts. *Catal. Sci. Technol.* **2013**, *3*, 1493–1496. [[CrossRef](#)]
98. Zahir, M.H.; Suzuki, T.; Fujishiro, Y.; Awano, M. Perovskites with cotton-like morphology consisting of nanoparticles and nanorods: Their synthesis by the combustion method and their NO_x adsorption behavior. *Appl. Catal. A Gen.* **2009**, *361*, 86–92. [[CrossRef](#)]
99. Du, S.; Wang, S.; Guo, Y.; Lu, X.; Tang, W.; Ding, Y.; Mao, X.; Gao, P. Rational design, synthesis and evaluation of ZnO nanorod array supported Pt: $\text{La}_{0.8}\text{Sr}_{0.2}\text{MnO}_3$ lean NO_x traps. *Appl. Catal. B Environ.* **2018**, *236*, 348–358. [[CrossRef](#)]
100. Alcalde-Santiago, V.; Davó-Quiñonero, A.; Such-Basáñez, I.; Lozano-Castelló, D.; Bueno-López, A. Macroporous carrier-free Sr-Ti catalyst for NO_x storage and reduction. *Appl. Catal. B Environ.* **2018**, *220*, 524–532. [[CrossRef](#)]
101. Wen, W.; Wang, X.; Jin, S.; Wang, R. LaCoO_3 perovskite in $\text{Pt}/\text{LaCoO}_3/\text{K}/\text{Al}_2\text{O}_3$ for the improvement of NO_x storage and reduction performances. *RSC Adv.* **2016**, *6*, 74046–74052. [[CrossRef](#)]
102. Onrubia-Calvo, J.A.; Pereda-Ayo, B.; Bermejo-López, A.; Caravaca, A.; Vernoux, P.; González-Velasco, J.R. Pd-doped or Pd impregnated 30% $\text{La}_{0.7}\text{Sr}_{0.3}\text{CoO}_3/\text{Al}_2\text{O}_3$ catalysts for NO_x storage and reduction. *Appl. Catal. B Environ.* **2019**, *259*, 118052. [[CrossRef](#)]
103. De-La-Torre, U.; Pereda-Ayo, B.; Onrubia, J.A.; González-Velasco, J.R. Effect of the Presence of Ceria in the NSR Catalyst on the Hydrothermal Resistance and Global De NO_x Performance of Coupled LNT-SCR Systems. *Top. Catal.* **2018**, *61*, 1993–2006. [[CrossRef](#)]
104. Seo, C.; Kim, H.; Choi, B.; Lim, M.T.; Lee, C.; Lee, C. De- NO_x characteristics of a combined system of LNT and SCR catalysts according to hydrothermal aging and sulfur poisoning. *Catal. Today* **2011**, *164*, 507–514. [[CrossRef](#)]
105. Nishihata, Y.; Mizuki, J.; Akao, T.; Tanaka, H.; Uenishi, M.; Kimura, M.; Okamoto, T.; Hamada, N. Self-regeneration of a Pd-perovskite catalyst for automotive emissions control. *Nature* **2002**, *418*, 164. [[CrossRef](#)] [[PubMed](#)]
106. Ohji, T.; Sekino, T.; Niihara, K. *The Science of Engineering Ceramics III*; Ceramics Society of Japan: Osaka, Japan, 2006; Volumes 317–318, p. 465.

107. Kinugasa, Y.; Igarashi, K.; Itou, T.; Suzuki, N.; Yaegashi, T.; Tanaka, T. Device for Purifying Exhaust Gas from Engine. U.S. Patent 5964088, 12 October 1999.
108. Gandhi, H.S.; Cavataio, J.V.; Hammerle, R.H.; Cheng, Y. Catalyst System for NO_x and NH₃. U.S. Patent 7332135, 19 December 2008.
109. Urrutxua, M.; Pereda-Ayo, B.; Trandafilovic, L.V.; Olsson, L.; González-Velasco, J.R. Influence of H₂, CO, C₃H₆, and C₇H₈ as Reductants on DeNO_x Behavior of Dual Monoliths for NO_x Storage/Reduction Coupled with Selective Catalytic Reduction. *Ind. Eng. Chem. Res.* **2019**, *58*, 7001–7013. [[CrossRef](#)]
110. Sakurai, K.; Miyashita, S.; Katumata, Y. Exhaust Purifying System for Internal Combustion Engine. U.S. Patent 2011/0214417 A1, 8 September 2011.
111. Sakurai, K. Exhaust Purifying System for Internal Combustion Engine. U.S. Patent 0138783 A1, 16 June 2011.
112. Onrubia-Calvo, J.A.; Pereda-Ayo, B.; De-La-Torre, U.; González-Velasco, J.R. Perovskite-Based Formulations as Rival Platinum Catalysts for NO_x Removal in Diesel Exhaust Aftertreatment. In *Perovskite Materials, Devices and Integration*; Tian, H., Ed.; Intechopen: London, UK, 2019.
113. Pereda-Ayo, B.; Duraiswami, D.; González-Velasco, J.R. Control of NO_x storage and reduction in NSR bed for designing combined NSR–SCR systems. *Catal. Today* **2011**, *172*, 66–72. [[CrossRef](#)]
114. De-La-Torre, U.; Pereda-Ayo, B.; Moliner, M.; González-Marcos, J.A.; Corma, A.; González-Velasco, J.R. Optimal Operating Conditions of Coupled Sequential NO_x Storage/Reduction and Cu/CHA Selective Catalytic Reduction Monoliths. *Top. Catal.* **2017**, *60*, 30–39. [[CrossRef](#)]



© 2020 by the authors. Licensee MDPI, Basel, Switzerland. This article is an open access article distributed under the terms and conditions of the Creative Commons Attribution (CC BY) license (<http://creativecommons.org/licenses/by/4.0/>).